

*Original article*

## Modelling and numerical simulation of martensitic transformation in shape memory alloys

M. Arndt<sup>1</sup>, M. Griebel<sup>1</sup>, T. Roubíček<sup>2,3</sup>

<sup>1</sup> Institut für Angewandte Mathematik, Rheinische Friedrich-Wilhelms-Universität Bonn,  
Wegeler Straße 6, 53115 Bonn, Germany

<sup>2</sup> Mathematical Institute, Charles University, Sokolovská 83, 186 75 Praha 8, Czech Republic

<sup>3</sup> Institute of Information Theory and Automation, Academy of Sciences,  
Pod vodárenskou věží 4, 182 08 Praha 8, Czech Republic

Received June 27, 2002 / Accepted March 18, 2003

Published online June 27, 2003 – © Springer-Verlag 2003

Communicated by S. Seelecke

**Abstract.** We consider the evolution of martensitic fine structures in shape memory alloys which undergo an isothermal phase-transformation. This process is modelled on a microscopical, continuum-mechanical level by partial differential equations. Here a homogeneous degree-1 dissipation potential is involved which can reflect specific energies needed for rate-independent phase transformations. An interface energy is incorporated by a nonlocal term, and hard-device loading is considered. After setting up the model and specifying its energy balance properties, three-dimensional numerical experiments for the cubic-to-tetragonal transformation in an InTi single crystal are presented which demonstrate geometrical/material interactions under tensile and shear loading.

**Key words:** shape-memory material, solid/solid phase transformation, multiwell stored energy, plastic-like dissipation, computer simulation

**MSC (2000):** 49S05, 74D10, 74N15, 74N30, 74S05

**PACS:** 81.30Kf

### 1 Introduction

Martensitic transformation in alloys, observed first around 1890 by the German microscopist Adolf Martens, has been intensively studied during the past decades. In physics and engineering there is increasing interest because of the ever-growing amount of applications, and in mathematics there has been an intensive research on this subject both theoretically and computationally. Several models of different kinds (single crystals/polycrystals, phenomenological/rigorously-based, atomic/continuum, microscopical/mesoscopical/macrosopical) have been proposed, analyzed and tested. Let us mention, without any ambitions for completeness, the models of Falk [23], Frémond [25,26], Idesman, Levitas and Stein [41], James [42], Lexcellent et al. [47,67], Mielke, Theil, and Levitas [52], Rajagopal and Srinivasa [66], or also [71]. Nevertheless, it seems that none of these models is fully capable to simulate the results of laboratory experiments on single-crystal specimens. Such experiments can be designed to observe the three-dimensional geometrical interactions of the loading device with the multiwell

structure of the specifically oriented single crystal and can exhibit both quite homogeneous deformations and resulting microstructure.

The starting point for a rigorous single-crystal model is the specific *stored energy density*  $\varphi : \mathbb{R}^{n \times n} \rightarrow \mathbb{R}$ . At any current location  $x$  we can write  $\varphi(\nabla u(x))$ , where  $u(x) = x + w(x)$  denotes the deformation while  $w : \Omega \rightarrow \mathbb{R}^n$  is the displacement considered on a reference body configuration  $\Omega \subset \mathbb{R}^n$ . Hence, the deformation gradient is  $\nabla u(x) = I + \nabla w$ , where  $I \in \mathbb{R}^{n \times n}$  denotes the identity matrix. In the context of *shape memory alloys* (SMA), this issue was thoroughly investigated by crystallographers and later also by mathematicians, in particular Ball and James [7,8], Bhattacharya, Firoozye, James, Kohn [9], Ericksen [21,22], Müller [57] and others. Falk [23] proposed a non-isothermal model which is based on Landau's theory. It involves the specific free energy density  $\varphi = \varphi(F, \vartheta)$ , which depends on the temperature  $\vartheta \in \mathbb{R}^+$ . A three-dimensional variant can be found in [24]. This model, augmented by capillarity- and viscosity-like terms, has been further studied e.g. by Garcke [28], Niezgodka and Sprekels [58], Hoffmann and Zochowski [38] and Pawłow [61], see also [12, Chap. 5] and the references therein.

In this paper, we confine ourselves to the isothermal situation  $\vartheta = \text{constant}$  which would correspond to a very slow experiment with a specimen kept on constant temperature by outer cooling. In this isothermal case, the class of models which consider only the stored energy density  $\varphi(F) = \varphi(F, \vartheta)$  (up to a constant) was investigated e.g. by Abeyaratne and Knowles [1], Andrews [5], Ball et al. [6], Dafermos [18], Friesecke and Dolzmann [27], Pego [62], Rybka [72], Rybka and Hoffmann [73], Swart and Holmes [78] or Truskinovsky [80]. However, it has been argued in [65] that such models cannot describe the rate-independent character of the activated phase-transformation process observed in experiments, which dissipates mechanical energy to some extent independently from the stored energy landscape  $\varphi$ . The complicated plastic-type dissipation mechanism is presumably activated by dislocation movement, thermal fluctuations, an interfacial energy at a "mesoscopic" phase-mixture level, by other phenomena or by their combination; cf. Miyazaki [26] or Müller et al. [39,40, 53–55]. Thus it seems inevitable that, at least on the level of continuum mechanics, this dissipation mechanism ought to be handled phenomenologically. The probably simplest approach to that relies on the prescription of the energy needed for the phase transformation. This is the approach used in our paper.

We consider the system of  $n$  semilinear equations

$$\varrho \frac{\partial^2 u}{\partial t^2} - \operatorname{div} (\sigma_{\text{plast}} + \sigma(\nabla u)) + \mu_1 \mathcal{A}_1 \frac{\partial u}{\partial t} + \mu_0 \mathcal{A}_0 u = f, \quad (1.1)$$

where  $\varrho$  is a mass density,  $\sigma = \varphi'$  is the elastic stress depending on the deformation gradient  $\nabla u$ ,  $\mu_1$  is a viscosity-like coefficient,  $\mu_0$  a capillarity-like coefficient,  $f$  is a body force, and  $\sigma_{\text{plast}}$  is a suitable additional stress reflecting the plastic, rate-independent character of the activated phase-transformation process like in classical plasticity, cf. eg. [43]. This  $\sigma_{\text{plast}}$  will be defined later in more detail, namely we will consider  $\sigma_{\text{plast}} = \sum_{\ell \in L} \sigma_\ell$  with  $\sigma_\ell$  from (2.21b). The linear operators  $\mathcal{A}_1$  and  $\mathcal{A}_0$  reflect viscosity-like and capillarity-like behavior, respectively, and must be given for concrete materials. They also serve as regularization terms to allow a rigorous analysis of the problem, to guarantee the energy balance (2.28) to be satisfied, and possibly to stabilize the calculations of the discrete scheme. Of course, the system (1.1) must be accompanied by suitable initial and boundary conditions. This model was basically proposed in [71, Formula (33)] and was further developed in [64] and [65] for  $\mathcal{A}_1 = \mathcal{A}_0 = \Delta^2$  and  $\mathcal{A}_1 = 0, \mathcal{A}_0 = \Delta^3$  respectively. It augments the conventional viscosity/capillarity-type models mentioned above which omit  $\sigma_{\text{plast}}$  and consider  $\mathcal{A}_1 = -\Delta$  and  $\mathcal{A}_0 = \Delta^2$ . It also admits either  $\mathcal{A}_1 = 0$  or  $\mathcal{A}_0 = 0$ .

In this paper we develop the above outlined model. Furthermore we present three-dimensional calculations with realistic data, which describe the martensitic transformation in an InTi shape memory alloy. Here we consider complex geometrical/material interactions for various loading experiments such as standard tensile or shear loading. To this end,  $\sigma_{\text{plast}}$  in the model (1.1) is designed to handle more complex dissipation mechanisms which describe transformations between many phases in one specimen. Moreover, contrary to [64], loading is achieved by time-dependent Dirichlet boundary conditions, so-called *hard device* loading, which are simpler to use in computational experiments and which are more realistic in connection with laboratory experiments. However, they require some care when specifying the energy balance, see (2.28) below. In contrast to (1.1), we neglect inertial forces, i.e.  $\varrho = 0$ , which is mathematically justified [64] and seems to be acceptable from the experimental point of view except for very fast loading regimes. Let us remark that the probably first attempt for stationary three-dimensional simulations for SMAs was accomplished by Collins and Luskin [17]. Evolutionary

three-dimensional simulations have been performed by Klouček and Luskin [44,45]. They however used a conventional model which, as explained in [65], cannot capture all desired phenomena.

The remainder of this paper is organized as follows: In Sect. 2 we set up the model and derive its energetics. Section 3 deals with the discretization and implementation of the model and discusses existence and convergence. In Sect. 4 we describe our computational experiments, and in Sect. 5 we give some concluding remarks.

## 2 The model

We will use the notation  $\Gamma$  for the boundary of the undeformed reference configuration  $\Omega \subset \mathbb{R}^n$  and  $\Gamma_0$  and  $\Gamma_1$  for the parts where Dirichlet and Neumann boundary conditions will be prescribed, respectively;  $\Gamma = \Gamma_0 \cup \Gamma_1$ ,  $\Gamma_0 \cap \Gamma_1 = \emptyset$ . For a fixed, finite time horizon  $T > 0$ , we denote  $Q = \Omega \times (0, T)$ ,  $\Sigma = \Gamma \times (0, T)$ ,  $\Sigma_i = \Gamma_i \times (0, T)$ ,  $i = 0, 1$ .

### 2.1 Stored energy: contribution from the deformation gradient

The stored energy density  $\varphi$  must be frame indifferent, i.e.  $\varphi(F) = \varphi(RF)$  for all  $R \in \text{SO}(n)$ , where  $\text{SO}(n)$  denotes the special orthogonal group of all orientation-preserving rotations. Besides,  $\varphi$  has a multi-well structure where each well (i.e. each local minimum of  $\varphi$ ) is an orbit of the form  $\text{SO}(n)U_\alpha$ ,  $\alpha = 1, \dots, N$ . Here  $N$  denotes the number of phases. Thus, each well corresponds to one so-called phase (in accordance with the convention in mathematical literature) or rather to a variant of a phase (as understood in physics). For example, the cubic phase (called austenite) has only one well, namely  $\text{SO}(n)$ . Tetragonal martensite has three variants, i.e. three wells, c.f. Sect. 4.1 below, while orthorhombic or monoclinic martensites have 6 or 12 wells, respectively.

It is usually a difficult task to determine the stored energy in a particular case with reasonable degree of reality. In general, it is difficult to describe the wells by means of atomic grid parameters, their energy in comparison with the other wells, and (at least approximately) their elastic properties. The InTi alloy modelled in Sect. 4.1 is an example where all these data are known.

### 2.2 Rate-independent dissipation

A crucial point is to adequately design the plastic-type dissipation mechanism. There exist a lot of phase transformation processes where each dissipates a different energy or, in other words, where each is activated by a different energy. To capture this in a general manner, we introduce indices  $\ell \in L$ , where

$$L \subset \{\ell \subset \{1, 2, \dots, N\} : \ell \neq \emptyset, \ell \neq \{1, 2, \dots, N\}\}. \quad (2.1)$$

Each  $\ell \in L$  identifies a nontrivial splitting of  $\{1, 2, \dots, N\}$ . For the reason of symmetry we can assume that for each  $\ell \in L$  we have  $\{1, 2, \dots, N\} \setminus \ell \notin L$ .

For each  $\ell \in L$  we introduce a continuous bounded function

$$\lambda_\ell : \mathbb{R}^{n \times n} \rightarrow \mathbb{R}, \quad (2.2)$$

which takes a constant value in a neighbourhood of the wells  $\text{SO}(n)U_\alpha$ ,  $\alpha \in \ell$ , and another constant value in a neighbourhood of the wells  $\text{SO}(n)U_\alpha$ ,  $\alpha \notin \ell$ . Therefore we call  $\lambda_\ell$  a *phase-transformation indicator*. Since  $1 \leq |L| \leq 2^N - 1$ , we might deal with up to three phase-transformation indicators for the transformations between three tetragonal martensitic phases. Even seven indicators may be considered for the transformations between one cubic austenite and three tetragonal martensite phases which occur at higher temperatures.

The energy needed for the transformation between two particular phases,  $\alpha$  and  $\beta$ , is therefore

$$\mathcal{E}_{\alpha\beta} = \sum_{\ell \in L} |\lambda_\ell(U_\alpha) - \lambda_\ell(U_\beta)|. \quad (2.3)$$

By choosing appropriate functions  $\lambda_\ell$ , this construction allows us to set up  $\mathcal{E}_{\alpha\beta}$  with great freedom.

The absolute value  $|\cdot|$  as a convex, non-negative, positively homogeneous function used in the formula (2.3) is known in plasticity-theory as a dissipation function. It determines the stress which activates the particular plastic process. Its subdifferential, see (2.22) below, has the important property to be a maximal responsive set-valued map (c.f. Eve, Reddy and Rockafellar [20] for details), which is intimately related to the principle of maximum plastic work (2.25) of Hill [37] (see also [50] or [51, 76]). The consequence of (2.3) is symmetry: the transformation from phase  $\alpha$  to phase  $\beta$  dissipates the same energy as the converse transformation.

### 2.3 Viscous-like damping and higher-order contributions to the stored energy

There is a high freedom to set up the operators  $\mathcal{A}_1$  and  $\mathcal{A}_0$  in (1.1). For simplicity we will consider  $\mathcal{A}_1 = \mathcal{A}_0 =: \mathcal{A}$ . This reflects the observation that every real mechanism which leads to the stored energy cannot be 100% efficient and necessarily dissipates (here in a viscous-like manner through the coefficient  $\mu_1$ ) a certain part of the energy. Though this is not necessary for the mere existence of a weak solution, it guarantees the energy balance (2.28). This would otherwise require a certain regularity of the solution which is not obvious because the plastic dissipative mechanism in (2.21a, 2.21b) involves a nonsmooth nonlinearity in a high mixed derivative. Besides,  $\mathcal{A}_1 = \mathcal{A}_0$  guarantees also the convergence of the numerical scheme. Let us remark that this does not cover the viscosity-capillarity model (see [1, 5, 18, 27, 62, 72, 73, 78]) which uses  $\mathcal{A}_1 = -\Delta u$  different from  $\mathcal{A}_0 = \Delta^2 u$ .

We derive the concrete form of  $\mathcal{A}$  from a nonnegative quadratic functional

$$a : L^2(\Omega; \mathbb{R}^{n \times n}) \rightarrow \mathbb{R} \cup \{+\infty\}, \quad (2.4)$$

which is in general finite only on a linear subspace of  $L^2(\Omega; \mathbb{R}^{n \times n})$ . We denote

$$\begin{aligned} L_a^2(\Omega; \mathbb{R}^{n \times n}) &:= \{z \in L^2(\Omega; \mathbb{R}^{n \times n}) : a(z) < +\infty\}, \\ W_a^{1,2}(\Omega; \mathbb{R}^n) &:= \{u \in W^{1,2}(\Omega; \mathbb{R}^n) : a(\nabla u) < +\infty\} \end{aligned} \quad (2.5)$$

and equip these linear spaces with the natural norms

$$\begin{aligned} \|z\|_{L_a^2(\Omega; \mathbb{R}^{n \times n})} &:= \left( \|z\|_{L^2(\Omega; \mathbb{R}^{n \times n})}^2 + a(z) \right)^{1/2}, \\ \|u\|_{W_a^{1,2}(\Omega; \mathbb{R}^n)} &:= \left( \|u\|_{W^{1,2}(\Omega; \mathbb{R}^n)}^2 + a(\nabla u) \right)^{1/2}, \end{aligned} \quad (2.6)$$

which makes them Hilbert spaces. A fundamental assumption on  $a$  is that it is coercive in such a compactifying manner that the following embedding holds:

$$L_a^2(\Omega; \mathbb{R}^{n \times n}) \subset L^2(\Omega; \mathbb{R}^{n \times n}) \quad \text{compactly.} \quad (2.7)$$

Now we define

$$\begin{aligned} \sigma_a &:= a' : L_a^2(\Omega; \mathbb{R}^{n \times n}) \rightarrow L_a^2(\Omega; \mathbb{R}^{n \times n})^*, \\ \mathcal{A} &:= (a \circ \nabla)' : W_a^{1,2}(\Omega; \mathbb{R}^n) \rightarrow W_a^{1,2}(\Omega; \mathbb{R}^n)^* \end{aligned} \quad (2.8)$$

to be the Gâteaux differentials of  $a$  and  $a \circ \nabla$  respectively. We have

$$\mathcal{A} = \nabla^* \circ \sigma_a \circ \nabla, \quad (2.9)$$

where  $\nabla^*$  denotes the adjoint operator of  $\nabla$ . Obviously  $\sigma_a$  and  $\mathcal{A}$  are linear operators. Furthermore we always have

$$a(\nabla u) = \frac{1}{2} \langle \mathcal{A}(u), u \rangle = \frac{1}{2} \langle \sigma_a(\nabla u), \nabla u \rangle, \quad (2.10)$$

where the first duality  $\langle \cdot, \cdot \rangle$  is between  $W_a^{1,2}(\Omega; \mathbb{R}^n)^*$  and  $W_a^{1,2}(\Omega; \mathbb{R}^n)$ , while the second one is between  $L_a^2(\Omega; \mathbb{R}^{n \times n})^*$  and  $L_a^2(\Omega; \mathbb{R}^{n \times n})$ .

*Example 1.* One possibility for the operator  $\mathcal{A}$  stems from the choice

$$a(z) := \frac{1}{2} \int_{\Omega} |\nabla z|^2 dx, \quad (2.11)$$

so we have  $W_a^{1,2}(\Omega; \mathbb{R}^n) \cong W^{2,2}(\Omega; \mathbb{R}^n)$ . Because  $\langle \sigma_a(z), \tilde{z} \rangle = \int_{\Omega} \nabla z \cdot \nabla \tilde{z} dx$ , we can symbolically write  $\sigma_a(\nabla u) = -\Delta \nabla u$  and  $\mathcal{A} = \operatorname{div} \operatorname{div} \nabla^2 u$ .

*Example 2.* Another example deals with a *nonlocal* energy in the form

$$a(z) := \frac{1}{4} \int_{\Omega} \int_{\Omega} K(x, \xi) \|z(x) - z(\xi)\|_{\mathbb{F}}^2 dx d\xi \quad (2.12)$$

with a symmetric, non-negative kernel  $K : \Omega \times \Omega \rightarrow \mathbb{R}$ . Here  $\|z\|_{\mathbb{F}} = \left( \sum_{ij} z_{ij}^2 \right)^{1/2}$  denotes the Frobenius norm of a matrix. Models of this type have been proposed in the case  $n = 1$  by Ren, Rogers, and Truskinovsky [68, 69] with either positive or also, for different purposes, non-positive kernels. The advantage of (2.12) in comparison with (2.11) is the following: Depending on the choice of  $K(x, \xi)$ , (2.12) can still have a compactifying effect on the deformation gradient, but it additionally might allow for sharp interfaces. This is in good agreement with experiments, where interfaces observed in SMAs are often atomically sharp [68]. Furthermore, this has also an advantage in the numerical treatment of the corresponding model: the diffuse interfaces arising from (2.11) are no longer present and we therefore need not resolve them on an unnecessarily fine grid.

Since we have

$$\frac{1}{2} \int_{\Omega} \int_{\Omega} K(x, \xi) (z(x) - z(\xi)) : (\tilde{z}(x) - \tilde{z}(\xi)) dx d\xi = \int_{\Omega} \int_{\Omega} K(x, \xi) (z(x) - z(\xi)) : \tilde{z}(x) dx d\xi \quad (2.13)$$

by symmetry of the kernel, the choice (2.12) results in the formula

$$[\sigma_a(z)](x) = \int_{\Omega} K(x, \xi) (z(x) - z(\xi)) d\xi \quad (2.14)$$

for the stress  $\sigma_a$ , see also [68, Formula (3.2)]. In particular we have

$$\int_{\Omega} \sigma_a(z) : z dx = \frac{1}{2} \int_{\Omega} \int_{\Omega} K(x, \xi) \|z(x) - z(\xi)\|_{\mathbb{F}}^2 dx d\xi = 2a(z), \quad (2.15)$$

compare (2.10).

An example for the kernel  $K$  is

$$K(x, \xi) = \frac{1}{|x - \xi|^{n+2\gamma}} \quad (2.16)$$

for a fixed parameter  $0 < \gamma < 1$ . Then  $W_a^{1,2}(\Omega; \mathbb{R}^n) \cong W^{1+\gamma,2}(\Omega; \mathbb{R}^n)$ , which enables us to employ the standard theory of Sobolev-Slobodeckii spaces  $W^{1+\gamma,2}(\Omega)$ . Later, we will use  $\gamma < 1/2$  to allow for sharp interfaces in the solution. Furthermore we will replace (2.16) by a wavelet-based kernel which leads to an equivalent norm but allows an efficient local implementation.

We require that

$$a(v) = 0 \quad \text{and} \quad v|_{\Gamma_0} = 0 \quad \text{implies} \quad v = 0. \quad (2.17)$$

This is fulfilled in both examples (2.11) and (2.12) if the interior of the convex hull of  $\Gamma_0$  is nonempty, since  $a(v) = 0$  implies that  $v$  is affine and affine functions are completely determined on  $\Gamma_0$  with such shape. We use this to derive the following Poincaré-like inequality.

**Lemma 2.1** *Let (2.7) and (2.17) hold. Then there is a constant  $C$  such that for all  $u \in W_a^{1,2}(\Omega; \mathbb{R}^n)$ :*

$$\|u\|_{W_a^{1,2}(\Omega; \mathbb{R}^n)}^2 \leq C(\|u\|_{L^2(\Gamma_0; \mathbb{R}^n)}^2 + a(\nabla u)). \quad (2.18)$$

*Proof.* Assume that for each  $k \in \mathbb{N}$  there exists  $u_k \in W_a^{1,2}(\Omega; \mathbb{R}^n)$  such that

$$1 = \|u_k\|_{W_a^{1,2}(\Omega; \mathbb{R}^n)}^2 > k(\|u_k\|_{L^2(\Gamma_0; \mathbb{R}^n)}^2 + a(\nabla u_k)). \quad (2.19)$$

Then  $\{u_k\}_{k \in \mathbb{N}}$  is bounded in  $W_a^{1,2}(\Omega; \mathbb{R}^n)$ . Since bounded subsets of  $W_a^{1,2}(\Omega; \mathbb{R}^n)$  are weakly sequentially compact, there exists a subsequence (also denoted by  $\{u_k\}_{k \in \mathbb{N}}$ ) which converges weakly to a function  $\bar{u} \in W_a^{1,2}(\Omega; \mathbb{R}^n)$ . The embedding  $W_a^{1,2}(\Omega; \mathbb{R}^n) \hookrightarrow W^{1,2}(\Omega; \mathbb{R}^n)$  is compact, so the subsequence also converges strongly to  $\bar{u}$  in  $W^{1,2}(\Omega; \mathbb{R}^n)$ . Because  $a \circ \nabla$  is weakly lower semicontinuous and  $a(\nabla u_k) \rightarrow 0$ , we have  $a(\nabla \bar{u}) = 0$ . Since  $u_k|_{\Gamma_0} \rightarrow \bar{u}|_{\Gamma_0}$  strongly in  $L^2(\Gamma_0; \mathbb{R}^n)$  and  $\|u_k\|_{L^2(\Gamma_0; \mathbb{R}^n)}^2 \rightarrow 0$ , we conclude  $\bar{u}|_{\Gamma_0} = 0$ . Because of (2.17) we have  $\bar{u} = 0$ . But

$$0 = \|\bar{u}\|_{W^{1,2}(\Omega; \mathbb{R}^n)}^2 = \lim_{k \rightarrow \infty} \|u_k\|_{W^{1,2}(\Omega; \mathbb{R}^n)}^2 = 1 - \lim_{k \rightarrow \infty} a(\nabla u_k) = 1 \quad (2.20)$$

is a contradiction.  $\square$

#### 2.4 The governing equations and inclusions

We now set up the governing initial-boundary-value problem. Starting from (1.1), we neglect the inertial term (i.e.  $\varrho = 0$ ) and take the desired plastic-type dissipated energy (2.3) and the regularizing contribution from the quadratic form  $a$  as discussed in Sect. 2.3 into account. Then, provided all functions are smooth enough and  $\sigma_a$  is pointwise defined, our problem reads in the classical formulation as follows:

$$- \operatorname{div} \left( \sum_{\ell \in L} \sigma_\ell + \sigma(\nabla u) + \sigma_a \left( \mu_1 \frac{\partial \nabla u}{\partial t} + \mu_0 \nabla u \right) \right) = f \quad \text{on } Q, \quad (2.21a)$$

$$\sigma_\ell \in \operatorname{sign} \left( \frac{\partial}{\partial t} \lambda_\ell(\nabla u) \right) \lambda'_\ell(\nabla u), \quad \ell \in L \quad \text{on } Q, \quad (2.21b)$$

$$u = u_D(x, t) \quad \text{on } \Sigma_0, \quad (2.21c)$$

$$\left( \sum_{\ell \in L} \sigma_\ell + \sigma(\nabla u) + \sigma_a \left( \mu_1 \frac{\partial \nabla u}{\partial t} + \mu_0 \nabla u \right) \right) \nu = g \quad \text{on } \Sigma_1, \quad (2.21d)$$

$$\text{natural boundary conditions arising from } a, \text{ e.g.} \quad (2.21e)$$

$$\begin{cases} (\nabla^2 u) \cdot \nu = 0 & \text{on } \Sigma \text{ in case of (2.11)} \\ \text{none} & \text{in case of (2.12),} \end{cases}$$

$$u(\cdot, 0) = u_0 \quad \text{on } \Omega. \quad (2.21f)$$

Here the set-valued mapping  $\operatorname{sign} : \mathbb{R} \rightrightarrows [-1, 1]$  is defined as usual by

$$\operatorname{sign}(\xi) := \begin{cases} 1 & \text{for } \xi > 0, \\ [-1, 1] & \text{for } \xi = 0, \\ -1 & \text{for } \xi < 0. \end{cases} \quad (2.22)$$

and  $\nu$  denotes the unit outward normal to  $\Gamma$ ,  $u_D$  denotes the prescribed displacement on the boundary  $\Gamma_1$ ,  $u_0$  the initial displacement, and  $\lambda'_\ell : \mathbb{R}^{n \times n} \rightarrow \mathbb{R}^{n \times n}$  denotes the differential of  $\lambda_\ell$ .

We now introduce new variables  $\omega_\ell \in \operatorname{sign}(\frac{\partial}{\partial t} \lambda_\ell(\nabla u))$  so that  $\sigma_\ell = \omega_\ell \lambda'_\ell(\nabla u)$ . They correspond to the direction of the transformation process which is associated with the index  $\ell$ . We multiply (2.21a) by a smooth test function  $v$ , integrate over  $Q$  and use Green's theorem. We then obtain the following weak formulation of the initial-boundary-value problem (2.21):

$$\int_0^T \int_\Omega \left( \sum_{\ell \in L} \omega_\ell \lambda'_\ell(\nabla u) + \sigma(\nabla u) \right) : \nabla v - f \cdot v \, dx,$$

$$-\int_{\Gamma_1} g \cdot v \, dS + \left\langle \sigma_a \left( \mu_1 \frac{\partial}{\partial t} \nabla u + \mu_0 \nabla u \right), \nabla v(\cdot, t) \right\rangle dt = 0 \quad (2.23a)$$

$$\forall v \in L^2(0, T; W_a^{1,2}(\Omega; \mathbb{R}^n)), \quad v|_{\Sigma_0} = 0,$$

$$\int_Q (\omega_\ell - z) \left( \lambda'_\ell(\nabla u) : \frac{\partial}{\partial t} \nabla u - v \right) dx \, dt \geq 0 \quad (2.23b)$$

$$\forall \ell \in L, v \in L^2(Q), z \in L^\infty(Q), z \in \text{sign}(v),$$

$$u|_{\Sigma_0} = u_D, \quad (2.23c)$$

$$u(\cdot, 0) = u_0. \quad (2.23d)$$

Here  $A : B = \sum_{i=1}^n \sum_{j=1}^m A_{ij} B_{ij}$  and  $u \cdot v = \sum_{j=1}^m u_j v_j$ , while  $\langle \cdot, \cdot \rangle$  in (2.23a) means the duality pairing between  $W_a^{1,2}(\Omega; \mathbb{R}^n)^*$  and  $W_a^{1,2}(\Omega; \mathbb{R}^n)$ .

Consequently, we call a  $(1 + |L|)$ -tuple  $(u, (\omega_\ell)_{\ell \in L})$  with  $u \in W^{1,2}(0, T; W_a^{1,2}(\Omega; \mathbb{R}^n))$  and  $\omega \in L^\infty(\Omega; \mathbb{R}^L)$  which fulfills (2.23) a weak solution of (2.21).

We ensure the integrability of all terms in (2.23) by the following data prerequisites:

$$\varphi \in C^1(\mathbb{R}^{n \times n}), \quad \varphi = \varphi_1 + \varphi_0 \quad \text{with } \varphi_1 \geq 0 \text{ convex}, \quad (2.24a)$$

$$\sigma_1 := \varphi'_1, \quad |\sigma_1(A)| \leq C(1 + |A|), \quad \sigma_0 := \varphi'_0 \text{ bounded},$$

$$\lambda_\ell \in W^{2,\infty}(\mathbb{R}^{n \times n}), \quad \ell \in L, \quad (2.24b)$$

$$u_D \in W^{1,2}(0, T; W_a^{1,2}(\Omega; \mathbb{R}^n)|_{\Gamma_0}), \quad (2.24c)$$

$$u_0 \in W_a^{1,2}(\Omega; \mathbb{R}^n), \quad u_0|_{\Gamma_0} = u_D|_{t=0}, \quad (2.24d)$$

$$f \in L^2(0, T; L^2(\Omega; \mathbb{R}^n)), \quad g \in L^2(0, T; L^2(\Gamma_1; \mathbb{R}^n)), \quad (2.24e)$$

$$\mu_1 > 0, \quad \mu_0 \geq 0. \quad (2.24f)$$

## 2.5 Energetics

From (2.23b) with  $v = 0$  we obtain

$$\frac{d\lambda_\ell(\nabla u)}{dt} \omega_\ell = \max_{\xi \in \text{sign}(0)} \frac{d\lambda_\ell(\nabla u)}{dt} \xi \quad \text{a.e. on } Q \quad (2.25)$$

for all transformation processes  $\ell \in L$ . This states that the dissipation of the transformation process  $\ell$  is maximal provided that the rate  $\frac{d}{dt} \lambda_\ell(\nabla u)$  is kept fixed while the direction  $\omega_\ell$  varies freely for all admissible directions with  $\text{sign}(0) = [-1, 1]$ . This just resembles Hill's maximum-dissipation principle, see [37, 50, 51] or [76]. In plasticity theory, this principle can alternatively be expressed as a normality in the sense that the rate of plastic deformation belongs to the cone of outward normals to the elasticity domain. Here, this would result in the observation that the rate  $\frac{d}{dt} \lambda_\ell(\nabla u)$  belongs to the normal cone of the interval  $[-1, 1]$  at the point  $\omega_\ell$ , i.e. to  $N_{[-1,1]}(\omega_\ell) := \partial \delta_{[-1,1]}(\omega_\ell)$ . As usual,  $\delta_{[-1,1]}$  denotes the indicator function of the interval  $[-1, 1]$  and  $\partial$  stands for the subdifferential.

However, the main justification of the model (2.21) is the following energy balance. Let

$$\sigma_{\text{tot}} \equiv \sigma_{\text{tot}}(u, (\omega_\ell)_{\ell \in L}) := \sum_{\ell \in L} \sigma_\ell + \sigma(\nabla u) + \sigma_a \left( \mu_1 \frac{\partial}{\partial t} \nabla u + \mu_0 \nabla u \right) \quad (2.26)$$

denote the total stress, where  $\sigma_\ell = \omega_\ell \lambda'_\ell(\nabla u)$ . Note that  $\sigma_\ell \in L^\infty(\Omega; \mathbb{R}^{n \times n})$ ,  $\sigma(\nabla u) \in L^2(\Omega; \mathbb{R}^{n \times n})$  and  $\sigma_a(\mu_1 \frac{\partial}{\partial t} \nabla u + \mu_0 \nabla u) \in L_a^2(\Omega)^*$ . Because  $L^\infty(\Omega; \mathbb{R}^{n \times n}) \subset L^2(\Omega; \mathbb{R}^{n \times n}) \cong L^2(\Omega; \mathbb{R}^{n \times n})^* \subset L_a^2(\Omega; \mathbb{R}^{n \times n})^*$  holds, we always have  $\sigma_{\text{tot}} \in L_a^2(\Omega; \mathbb{R}^{n \times n})^*$ . Since in our general context  $\sigma_a$  may not be pointwise defined, we cannot simply restrict it to the boundary to define the normal stress. Instead we define  $\sigma_\nu \in (W_a^{1,2}(\Omega; \mathbb{R}^n)|_{\Gamma_0})^*$  by means of

$$\langle \sigma_\nu, v|_{\Gamma_0} \rangle = \langle \sigma_{\text{tot}}, \nabla v \rangle - \int_\Omega f \cdot v \, dx - \int_{\Gamma_1} g \cdot v \, dS \quad \forall v \in W_a^{1,2}(\Omega; \mathbb{R}^n). \quad (2.27)$$

Let us remark that the definition of the normal stress holds only for a solution of (2.23) and not an arbitrary function  $(u, (\omega_\ell)_{\ell \in L})$ . Due to (2.23a) the normal stress is independent of the actual extension  $v$  of  $v|_{\Gamma_0}$  and is therefore well-defined.

**Proposition 2.2** *If (2.24) holds, then any weak solution  $(u, (\omega_\ell)_{\ell \in L})$  of (2.21) satisfies the following energy balance:*

$$\begin{aligned} \Phi(u(\cdot, T)) + \int_{\Omega} \sum_{\ell \in L} \text{Var}_{t \in [0, T]} \lambda_\ell(\nabla u(x, t)) \, dx + 2\mu_1 \int_0^T a \left( \frac{\partial \nabla u}{\partial t} \right) \, dt \\ = \Phi(u_0) + \int_0^T \left( \left\langle \sigma_\nu, \frac{\partial u_D}{\partial t} \right\rangle + \int_{\Omega} f \cdot \frac{\partial u}{\partial t} \, dx + \int_{\Gamma_1} g \cdot \frac{\partial u}{\partial t} \, dS \right) \, dt. \end{aligned} \quad (2.28)$$

Here  $\text{Var}$  denotes the total variation of a real-valued function over the indicated time interval and

$$\Phi(u) = \int_{\Omega} \varphi(\nabla u) \, dx + \mu_0 a(\nabla u) \quad (2.29)$$

gives the total stored energy. The particular terms in (2.28) denote successively:

- the total stored energy at time  $t = T$ ,
- the total energy dissipated due to the phase transformation,
- the energy dissipated by viscous-like damping,
- the total stored energy at time  $t = 0$ ,
- the work due to the displacement  $u_D$  over the time interval  $[0, T]$ ,
- the work due to the body force  $f$  over the time interval  $[0, T]$ , and
- the work due to the surface force  $g$  over the time interval  $[0, T]$ .

*Proof.* As  $\omega_\ell \in \text{sign}(\frac{\partial}{\partial t} \lambda_\ell(\nabla u))$  a.e., we have the following identity for the dissipation rate related to all phase transformations:

$$r(u) := \sum_{\ell \in L} \sigma_\ell : \frac{\partial \nabla u}{\partial t} = \sum_{\ell \in L} \omega_\ell \lambda'_\ell(\nabla u) : \frac{\partial \nabla u}{\partial t} = \sum_{\ell \in L} \omega_\ell \frac{\partial}{\partial t} \lambda_\ell(\nabla u) = \sum_{\ell \in L} \left| \frac{\partial}{\partial t} \lambda_\ell(\nabla u) \right|. \quad (2.30)$$

As  $u \in W^{1,2}(0, T; W_a^{1,2}(\Omega; \mathbb{R}^n))$ , we can put  $v = \frac{\partial}{\partial t}(u - \bar{u}_D) \in L^2(0, T; W_a^{1,2}(\Omega; \mathbb{R}^n))$  into (2.23a), where we denote by  $\bar{u}_D \in W^{1,2}(0, T; W_a^{1,2}(\Omega; \mathbb{R}^n))$  an extension of  $u_D$  onto  $Q$ , i.e.  $\bar{u}_D|_{\Sigma_0} = u_D$ . In this way we ensure  $v|_{\Sigma_0} = 0$ , hence  $v$  is indeed a legal test function for (2.23a). Then, using (2.27),  $\langle \sigma_a(\frac{\partial}{\partial t} \nabla u), \frac{\partial}{\partial t} \nabla u \rangle = 2a(\frac{\partial}{\partial t} \nabla u)$  (cf. (2.10)) and  $\langle \sigma_a(\nabla u), \frac{\partial}{\partial t} \nabla u \rangle = \frac{\partial}{\partial t} a(\nabla u)$ , we obtain

$$\begin{aligned} \int_0^T \left( \int_{\Omega} (r(u) + \frac{\partial}{\partial t} \varphi(\nabla u) - f \cdot \frac{\partial u}{\partial t}) \, dx - \int_{\Gamma_1} g \cdot \frac{\partial u}{\partial t} \, dS + 2\mu_1 a \left( \frac{\partial \nabla u}{\partial t} \right) + \mu_0 \frac{\partial}{\partial t} a(\nabla u) \right) \, dt \\ = \int_0^T \left( \int_{\Omega} \left( \sum_{\ell \in L} \sigma_\ell + \sigma(\nabla u) \right) : \frac{\partial \nabla \bar{u}_D}{\partial t} - f \cdot \frac{\partial \bar{u}_D}{\partial t} \, dx \right. \\ \left. - \int_{\Gamma_1} g \cdot \frac{\partial \bar{u}_D}{\partial t} \, dS + \left\langle \sigma_a \left( \mu_1 \frac{\partial}{\partial t} \nabla u + \mu_0 \nabla u \right), \frac{\partial \nabla \bar{u}_D}{\partial t} \right\rangle \right) \, dt \\ = \int_0^T \left( \left\langle \sigma_{\text{tot}}, \frac{\partial \nabla \bar{u}_D}{\partial t} \right\rangle - \int_{\Omega} f \cdot \frac{\partial \bar{u}_D}{\partial t} \, dx - \int_{\Gamma_1} g \cdot \frac{\partial \bar{u}_D}{\partial t} \, dS \right) \, dt \\ = \int_0^T \left\langle \sigma_\nu, \frac{\partial u_D}{\partial t} \right\rangle \, dt. \end{aligned} \quad (2.31)$$

This implies equality (2.28).  $\square$



### 3 The discretization and implementation of the model

In this section we describe the discretization of the model based on conformal finite-elements in space and an implicit Euler formula in time. The convergence proof is outlined in Sect. 3.4. Furthermore we discuss the recursive minimization problem created by the implicit time discretization. Finally, we present an efficient treatment of energies with a nonlocal term like (2.16) in (2.12).

We emphasize that a numerical simulation based on the model from Sect. 2 is quite demanding because of its complexity and nonlinearity. A successful treatment requires to handle the model with full rigor not to destroy its energetics as given in Sect. 2.5. Note that due to possible shock waves, the energy balance (2.28) may hold only as an inequality “<” if the quadratic form  $a$  does not have the compactifying character of (2.7), c.f. [80].

#### 3.1 The space and time discretization

For the space discretization we use finite elements. Then, a conformal discretization of the higher order term  $a$  for the conventional capillarity (2.11) requires higher-order finite elements. This approach is followed in [63] for  $d = 1$  and partly in [45] for  $d = 3$ . In the latter article the authors use the Adini-Clough-Melosh element. Note however that they cannot fully guarantee the embedding of the finite-element space into the energy space  $W_a^{1,2}(\Omega; \mathbb{R}^n) = W^{2,2}(\Omega; \mathbb{R}^n)$ . Also, rate-independent terms were not considered there.

The fourth order term (2.11) has the following disadvantage: It requires an extremely fine mesh to resolve the diffuse interfaces. Otherwise the microstructure pattern would be smeared out completely. But remember that it was merely introduced to regularize the model by its compactifying character. Therefore we will use the term (2.12), i.e.

$$a(z) := \frac{1}{4} \int_{\Omega} \int_{\Omega} K(x, \xi) \|z(x) - z(\xi)\|_{\mathbb{F}}^2 dx d\xi$$

in the following. With a kernel  $K$  of the type (2.16), we obtain the fractional order seminorm  $a(\nabla u) = |u|_{W^{1+\gamma,2}(\Omega; \mathbb{R}^n)}^2$ , which is compactifying iff  $\gamma > 0$ . We will furthermore choose  $\gamma < 1/2$ . This allows us to use piecewise linear and globally continuous finite elements, since they are then contained in the energy space  $W_a^{1,2}(\Omega; \mathbb{R}^n) = W^{1+\gamma,2}(\Omega; \mathbb{R}^n)$ .

The discretization is done separately in space and time. For the spatial discretization, let us assume that  $\Omega$  is polyhedral. For each mesh parameter  $h > 0$ , consider a finite decomposition  $\mathcal{T}_h$  of  $\Omega$  into tetrahedra whose diameters do not exceed  $h$ . Let

$$V_h = \{v_h \in W_a^{1,\infty}(\Omega; \mathbb{R}^n) : v_h|_T \text{ affine } \forall T \in \mathcal{T}_h\} \quad (3.1)$$

denote the finite-dimensional space of elementwise affine functions from  $W_a^{1,2}(\Omega; \mathbb{R}^n)$ , and let

$$L_h = \{\omega_h \in L^\infty(\Omega; \mathbb{R}^L) : \omega_h|_T \text{ constant } \forall T \in \mathcal{T}_h\} \quad (3.2)$$

denote the finite-dimensional space of elementwise constant functions from  $L^\infty(\Omega; \mathbb{R}^L)$ . We assume that  $\bigcup_{h>0} V_h$  is dense in  $W_a^{1,2}(\Omega; \mathbb{R}^n)$  and that the meshes are nested, i.e.  $V_{h_1} \subset V_{h_2}$  for  $h_1 \geq h_2 > 0$ . We also assume that all meshes are consistent with the splitting  $\Gamma = \Gamma_0 \cup \Gamma_1$ .

By means of the time discretization, we want to obtain a time-recursive sequence of problems which will later be solved by an implicit Euler method. To this end, let  $\tau > 0$  denote the discrete time step and assume that  $T/\tau$  is an integer. Now we consider the discrete solution at the time steps  $\tau, 2\tau, \dots, T$ . Thus we deal with a finite sequence

$$((u_{h\tau}^k, \omega_{h\tau}^k))_{k=1}^{T/\tau} \quad \text{with} \quad (u_{h\tau}^k, \omega_{h\tau}^k) \in V_h \times L_h. \quad (3.3)$$

To satisfy the boundary conditions we additionally require

$$u_{h\tau}^k|_{\Gamma_0} = u_D(\cdot, k\tau) \quad (3.4)$$

to hold.

For fixed  $h > 0$  and  $\tau > 0$ , this discretization of (2.23) leads straightforwardly to the recursive scheme:  
For  $k = 0$  set

$$u_{h\tau}^0 = u_0. \quad (3.5)$$

For  $k = 1, 2, \dots, T/\tau$  find  $(u_{h\tau}^k, \omega_{h\tau}^k)$  such that

$$\begin{aligned} \int_{\Omega} \left( \sum_{\ell \in L} \omega_{h\tau, \ell}^k \lambda'_{\ell}(\nabla u_{h\tau}^k) + \sigma(\nabla u_{h\tau}^k) \right) : \nabla v_h - f_{\tau}^k \cdot v_h \, dx \\ - \int_{\Gamma_1} g_{\tau}^k \cdot v_h \, dS + \left\langle \sigma_a \left( \mu_1 \frac{\nabla u_{h\tau}^k - \nabla u_{h\tau}^{k-1}}{\tau} + \mu_0 \nabla u_{h\tau}^k \right), \nabla v_h \right\rangle = 0 \end{aligned} \quad (3.6)$$

for all  $v_h \in V_h$  with  $v_h|_{\Gamma_0} = 0$  and

$$\int_{\Omega} (\omega_{h\tau, \ell}^k - z) \left( \frac{\lambda_{\ell}(\nabla u_{h\tau}^k) - \lambda_{\ell}(\nabla u_{h\tau}^{k-1})}{\tau} - v \right) dx \geq 0 \quad (3.7)$$

for all  $\ell = 1, \dots, L$ ,  $v \in L^2(\Omega)$  and  $z \in L^{\infty}(\Omega)$  with  $z \in \text{sign}(v)$ .

Here we used the abbreviations

$$f_{\tau}^k := \frac{1}{\tau} \int_{(k-1)\tau}^{k\tau} f(\cdot, t) \, dt \quad \text{and} \quad g_{\tau}^k := \frac{1}{\tau} \int_{(k-1)\tau}^{k\tau} g(\cdot, t) \, dt. \quad (3.8)$$

Later in the convergence proof (see Sect. 3.4) we will consider the piecewise affine interpolation of  $\{u_{h\tau}^k\}_k$  in time and the piecewise constant interpolation of  $\{\omega_{h\tau}^k\}_k$  in time to imbed the discrete solutions into the space of the continuous solutions.

### 3.2 Solution of the implicit scheme

Now, the recursive system of the nonlinear equation (3.6) coupled with the variational inequality (3.7) must be solved numerically for  $k = 1, 2, \dots, T/\tau$ . To this end we proceed as follows: Note that both  $\sigma$  and  $\sigma_a$  have potentials. Therefore we can rewrite problem (3.6) as a nonconvex minimization problem at each time level  $k$ :

$$\begin{aligned} \text{Minimize } E_{h\tau}^k(u) = \int_{\Omega} \varphi(\nabla u) + \tau \sum_{\ell \in L} \left| \frac{\lambda_{\ell}(\nabla u) - \lambda_{\ell}(\nabla u_{h\tau}^{k-1})}{\tau} \right| - f_{\tau}^k \cdot u \, dx \\ + \tau \mu_1 a \left( \frac{\nabla u - \nabla u_{h\tau}^{k-1}}{\tau} \right) + \mu_0 a(\nabla u) - \int_{\Gamma_1} g_{\tau}^k \cdot u \, dS \Bigg\}. \end{aligned} \quad (3.9)$$

subject to  $u \in V_h$ ,  $u|_{\Gamma_0} = u_D(\cdot, k\tau)$

We believe that this approach imitates the behaviour of nature where also minimization at least on a local scale is relevant.

A compactness and coercivity argument shows that the discrete minimization problem (3.9) has at least one solution. Without going further into technical details, let us mention that the functional  $E_{h\tau}^k$  is locally Lipschitz-continuous. Consequently, any local minimizer must satisfy the necessary first-order optimality condition that Clarke's generalized gradient contains an element perpendicular to  $\{v \in V_h; v|_{\Gamma_0} = 0\}$ , see also [15]. The reader not familiar with the concept of generalized gradients can equally imagine the following: Smooth the absolute value in (3.9), derive standard smooth optimality conditions, and then pass to the nonsmooth limit case, cf. also [63]. In any case, this results precisely in (3.6) and (3.7).

The choice of a minimization algorithm to solve (3.9) is a delicate point because of non-convexity, non-smoothness and high dimensionality. Here we tested two methods: the simple steepest descent approach (see e.g. [48]) and the conjugate gradient method by Fletcher/Reeves (see [29]). Both algorithms are implemented in

such a way that they choose one element from the generalized gradient and then act like in the smooth case. It turned out that this strategy works reliably in all our numerical experiments.

The steepest descent method can briefly be described by

$$\begin{aligned} d^j &:= [E_{h\tau}^k]'(u^j), \\ u^{j+1} &:= u^j - \alpha^j d^j \end{aligned} \quad (3.10)$$

for  $j = 0, 1, 2, \dots$ , where  $[\cdot]'$  denotes one element of the generalized gradient. The Fletcher/Reeves variant of the conjugate gradient algorithm is given by

$$\begin{aligned} d^j &:= [E_{h\tau}^k]'(u^j) + \frac{\| [E_{h\tau}^k]'(u^j) \|_2^2}{\| [E_{h\tau}^k]'(u^{j-1}) \|_2^2} d^{j-1}, \\ u^{j+1} &:= u^j - \alpha^j d^j \end{aligned} \quad (3.11)$$

for  $j = 0, 1, 2, \dots$  with the initial definition  $d^{-1} := 0$ . The step size  $\alpha^j$  is determined in both cases similarly to the Armijo method:

$$\begin{aligned} \alpha^{-1} &:= 1, \\ \alpha^j &:= \alpha^{j-1} \max\{2^i : i \in \mathbb{Z} \text{ and } \forall j \in [\min(0, i), i] \cap \mathbb{Z} : \\ &E_{h\tau}^k(u^j - 2^j \alpha^{j-1} d^j) \leq E_{h\tau}^k(u^j) - \beta 2^j \alpha^{j-1} d^j \cdot [E_{h\tau}^k]'(u^j)\}, \end{aligned} \quad (3.12)$$

where  $\beta \in (0, 1)$  is a fixed parameter. For deriving the inequality in (3.12), we start with the first-order Taylor expansion of  $E_{h\tau}^k$  (at least in the smooth case):

$$E_{h\tau}^k(u^j - 2^j \alpha^{j-1} d^j) = E_{h\tau}^k(u^j) - 2^j \alpha^{j-1} d^j \cdot [E_{h\tau}^k]'(u^j) + \text{h.o.t.} \quad (3.13)$$

Neglecting the higher order terms, we cannot expect that this equality holds for any step size. But for sufficiently small step sizes and smooth  $E_{h\tau}^k$  we always have

$$E_{h\tau}^k(u^j - 2^j \alpha^{j-1} d^j) \leq E_{h\tau}^k(u^j) - \beta 2^j \alpha^{j-1} d^j \cdot [E_{h\tau}^k]'(u^j). \quad (3.14)$$

Therefore (3.12) means that the new step size  $\alpha^j$  is determined from the old step size  $\alpha^{j-1}$  by doubling it as long as the condition (3.14) holds or halving it until (3.14) holds. The whole process is repeated until  $\alpha^j$  gets too small or  $j$  exceeds a predefined limit.

The steepest descent method turned out to perform much better than the conjugate gradient method. This is in good agreement with the observations in [17] where basically our problem without viscosity and capillarity was dealt with for the special smooth case  $\lambda_\ell \equiv 0$ . This higher efficiency of the first, lower-order method might be explained by the highly oscillating second (and even first) derivative of the energy functional, which makes the orthogonalization of the search directions with respect to the second derivative questionable.

### 3.3 Implementation of nonlocal terms

As mentioned above, we chose (2.12) with the kernel (2.16) for the operator  $\mathcal{A}$ . After discretizing the function space  $V$  to  $V_h$  as described in Sect. 3.1 and passing to the minimization problem as described in Sect. 3.2 we end up with a double integral. Since the integral kernel is nonlocal, a straightforward implementation would have a complexity of the order  $O(h^{-6})$  for the three-dimensional case. This is computationally too expensive, and we have to resort to a less expensive approach.

There are many different fields in which similar problems occur. One is the computation of long range forces in  $N$ -body problems from astrophysics and molecular dynamics. Here the Barnes-Hut algorithm (see [36]) or the fast multipole method by Greengard and Rokhlin (see [30–32]) reduce the  $O(N^2)$  complexity of the naive direct computation substantially. Another way is to utilize the panel clustering technique of Hackbusch and Nowak (see [35,74]), which stems from the area of boundary element methods. It is closely related to the so-called  $\mathcal{H}$ -matrices of Hackbusch, see [34]. Furthermore, the skeleton method of Tyrtysnikov (see [81]) provides a way

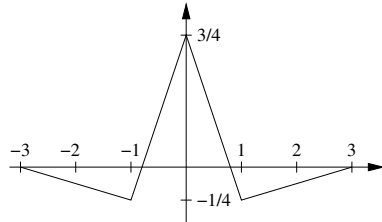
to deal with matrices which come from asymptotically smooth functions like our kernel. Finally one might follow Brandt and split the kernel into a local and a smooth long range part and then perform a multilevel summation, see [10,11]. All these approaches can be adapted to our setting. They result in an algorithm with a complexity of the order  $O(h^{-3}(\log h^{-1})^\alpha)$  on the expense of an approximation to the exact result with prescribed error. Hereby  $\alpha$  depends on the respective approach.

In the following we chose another way to reduce the complexity which utilizes wavelets (see [75]). In principle it works as follows: Consider the wavelet representation of the function  $u_h \in V_h$ . It is well known that a weighted  $\ell_2$ -norm of the wavelet coefficients is equivalent up to constants to the norm  $\|u_h\|_{W^{1+\gamma,2}}$ . By means of a Poincaré-like inequality we obtain equivalency to  $a(\nabla u_h)$ . The idea is now to approximate  $a(\nabla u_h)$  by the weighted  $\ell_2$ -norm of the associated wavelet coefficients. This is clearly not an equality, but the qualitative behaviour of the  $a$ -term is retained, such as the compactifying character which it was introduced for. The wavelet transformation can be performed with complexity  $O(h^{-3})$ , so that this approach finally leads to an  $O(h^{-3})$  algorithm.

Let us go into details. The multivariate wavelet transformation on a simplicial grid is possible but difficult, see [19]. Therefore we use a tensor product ansatz to further simplify things. First, consider the univariate case  $n = 1$ . The wavelet representation of a function  $u_h \in V_h(I)$  defined on an interval  $I$  is given as

$$u_h(x) = \sum_{l=0}^L \sum_k u_h^{l,k} \psi^{l,k}(x). \tag{3.15}$$

Here  $u_h^{l,k} \in \mathbb{R}$  denote the wavelet coefficients, the subscript  $l$  indicates the dilatation and  $k$  the translation of a mother wavelet  $\psi$ .<sup>1</sup> The maximal level  $l$  is denoted by  $L$  and depends on  $h$ . We chose the following mother wavelet which comes from the lifting scheme, cf. [79]:

$$\psi(x) = \begin{cases} -\frac{1}{8}x - \frac{3}{8} & \text{if } x \in [-3, -1], \\ x + \frac{3}{4} & \text{if } x \in [-1, 0], \\ -x + \frac{3}{4} & \text{if } x \in [0, 1], \\ \frac{1}{8}x - \frac{3}{8} & \text{if } x \in [1, 3], \\ 0 & \text{otherwise.} \end{cases} \tag{3.16}$$


It is well known (see [46, p. 16] or [60]) that the norm equivalence

$$\|u_h\|_{W^{1,2}(I)}^2 + a(\nabla u_h) = \|u_h\|_{W^{1+\gamma,2}(I)}^2 \cong \sum_{l=0}^L 4^{(1+\gamma)l} \sum_k |u_h^{l,k}|^2 \|\psi^{l,k}\|_{L^2(I)}^2 \tag{3.17}$$

holds within a certain range of  $\gamma$ , which depends on the special choice of the wavelets, here  $\gamma \in (-1.171, 0.5)$ , cf. [46, p. 24]. The involved constants are independent of  $h$ . Since we are interested in  $a(\nabla u_h)$  and not in  $\|u_h\|_{W^{1+\gamma,2}(I)}^2$ , we have to get rid of the term  $\|u_h\|_{W^{1,2}(I)}^2$ . A small modification of Lemma 2.1 shows that  $\|\cdot\|_{W^{1+\gamma,2}(I)}^2 \cong a \circ \nabla$  if we restrict us to a closed subspace of  $W^{1+\gamma,2}(I)$  which does not contain the affine functions (except the zero function of course). Hence we project out the affine functions and pass over to  $a \circ \nabla$ .

It turns out to be handy to use the  $L^2$ -orthogonal projection  $P$  to remove the affine functions. The wavelets we use have two vanishing moments. Thus all  $\psi^{l,k}$  with  $l \geq 1$  are  $L^2$ -orthogonal to the affine functions. The space of affine functions is exactly  $\text{span}\{\psi^{0,k}\}$ . Consequently the wavelet representation of  $Pu_h$  is the wavelet representation of  $u_h$  with the coefficients  $u_h^{0,k}$  set to zero, and we have

$$a(\nabla u_h) = a(\nabla Pu_h) \cong \sum_{l=1}^L 4^{(1+\gamma)l} \sum_k |u_h^{l,k}|^2 \|\psi^{l,k}\|_{L^2(I)}^2. \tag{3.18}$$

<sup>1</sup> Further modifications are necessary near the boundary, see [79].

To extend this to the multivariate case, we perform a tensor product type splitting

$$\begin{aligned} W^{1+\gamma,2}(I^n) &= W^{1+\gamma,2}(I) \otimes L^2(I) \otimes L^2(I) \otimes \dots \otimes L^2(I) \\ &\cap L^2(I) \otimes W^{1+\gamma,2}(I) \otimes L^2(I) \otimes \dots \otimes L^2(I) \\ &\cap \dots \\ &\cap L^2(I) \otimes \dots \otimes L^2(I) \otimes W^{1+\gamma,2}(I) \end{aligned} \quad (3.19)$$

with the corresponding norm equivalence

$$\|u_h\|_{W^{1+\gamma,2}(I^n)}^2 \cong \sum_{l \in \{0,1,2,\dots,L\}^n} 2^{2(1+\gamma)|l|_\infty} \sum_k |u_h^{l,k}|^2 \|\psi^{j,k}\|_{L^2(I^n)}^2. \quad (3.20)$$

We filter the affine functions and replace  $a(u_h)$  by the resulting expression similar to the right hand side of (3.18) for the numerical calculations.

Of course, the tensor product ansatz poses a restriction on the domain and on the grid. Since our simulations are based on a cubic domain anyway, this causes no disadvantage.<sup>2</sup> Furthermore the tensor product leads to a new finite element space, namely piecewise multilinear functions on cubes instead of piecewise linear functions on simplices. But note that the nodewise interpolation between these FE spaces is a bijective mapping. Furthermore the resulting seminorms are equivalent with constants independent on  $h$ . Hence our simple tensor product approach only introduces a further constant to our approximation like the one in the first norm equivalence and is therefore acceptable.

Both the wavelet transformation and the inverse wavelet transformation (which is needed to compute the gradient of the functional for the minimization routine) can be computed with  $O(h^{-3})$  operations. Thus we finally get an algorithm with the overall complexity  $O(h^{-3})$  for the computation of an approximation of the term  $a(\nabla u)$  and its derivative.

### 3.4 The convergence analysis

Now, after the discussion of the solution procedure and implementational details, we sketch the convergence analysis of the recursive scheme. To this end, we assume that the extension  $\bar{u}_D$  of  $u_D$  (cf. the proof of Proposition 2.2) is piecewise affine in time for all considered times steps  $\tau > 0$ . Furthermore,  $\bar{u}_D$  should belong to  $C(0, T; V_h)$ , which is not a restrictive assumption from the viewpoint of Sect. 4.2.

It was already mentioned in Sect. 3.2 that each arising discrete problem always possesses a solution. Now we study the convergence of the solutions of the discrete problems. In particular we obtain the existence of a solution of the continuous problem. Recall that the solution of (3.6) and (3.7) (which may not be unique) was denoted by  $\{(u_{h\tau}^k, \omega_{h\tau}^k)\}_{k=0\dots T/\tau}$ . By  $u_{h\tau}$  we denote its piecewise affine and by  $\bar{u}_{h\tau}$  its piecewise constant interpolation in time, i.e.  $u_{h\tau}^k = u_{h\tau}(k\tau) = \bar{u}_{h\tau}|_{((k-1)\tau, k\tau]}$ . The term  $\bar{\omega}_{h\tau}$  is defined analogously.

**Proposition 3.1** *Let (2.7), (2.17) and (2.24) hold and let  $\tau$  be small enough. Then there exists a constant  $C$  which is independent of  $h$  and  $\tau$  so that we have for all approximate solutions  $u_{h\tau}$  of (3.6) the a priori estimate*

$$\|u_{h\tau}\|_{W^{1,2}(0,T;W_a^{1,2}(\Omega;\mathbb{R}^n))} \leq C. \quad (3.21)$$

*Proof.* We test (3.6) with  $v_h = u_{h\tau}^k - u_{h\tau}^{k-1} - \tau \frac{\partial}{\partial t} \bar{u}_D$ . Using the convexity of  $\varphi_1$ , the growth conditions (2.24a) on  $\sigma_0$  and  $\sigma_1$  and Poincaré-like inequalities we obtain the estimate

$$\begin{aligned} &\int_{\Omega} \varphi_1(\nabla u_{h\tau}^k) - \varphi_1(\nabla u_{h\tau}^{k-1}) \, dx + 2\tau\mu_1 a \left( \frac{\nabla u_{h\tau}^k - \nabla u_{h\tau}^{k-1}}{\tau} \right) + \mu_0 a(\nabla u_{h\tau}^k) - \mu_0 a(\nabla u_{h\tau}^{k-1}) \\ &\leq \int_{\Omega} \sigma_1(\nabla u_{h\tau}^k) : (\nabla u_{h\tau}^k - \nabla u_{h\tau}^{k-1}) \, dx + \left\langle \sigma_a \left( \mu_1 \frac{\nabla u_{h\tau}^k - \nabla u_{h\tau}^{k-1}}{\tau} + \mu_0 \nabla u_{h\tau}^k \right), \nabla u_{h\tau}^k - \nabla u_{h\tau}^{k-1} \right\rangle \end{aligned}$$

<sup>2</sup> Note that for the case of a more general shape of the domain we could follow [19].

$$\begin{aligned}
&\leq \tau \int_{\Omega} \sigma_1(\nabla u_{h\tau}^k) : \frac{\partial}{\partial t} \nabla \bar{u}_D - \left[ \sigma_0(\nabla u_{h\tau}^k) + \sum_{\ell \in L} \omega_{h\tau\ell}^k \lambda'_\ell(\nabla u_{h\tau}^k) \right] : \left[ \nabla u_{h\tau}^k - \nabla u_{h\tau}^{k-1} - \tau \frac{\partial}{\partial t} \nabla \bar{u}_D \right] \\
&\quad + f_{h\tau}^k \cdot [u_{h\tau}^k - u_{h\tau}^{k-1} - \tau \bar{u}_D] \, dx \\
&\quad + \int_{\Gamma_1} g_{h\tau}^k \cdot [u_{h\tau}^k - u_{h\tau}^{k-1} - \tau \bar{u}_D] \, dS + \left\langle \sigma_a \left( \mu_1 \frac{\nabla u_{h\tau}^k - \nabla u_{h\tau}^{k-1}}{\tau} + \mu_0 \nabla u_{h\tau}^k \right), \tau \frac{\partial}{\partial t} \nabla \bar{u}_D \right\rangle \\
&\leq C\tau \left( 1 + \frac{1}{\delta} \right) + \tau^2 \delta \sum_{i=1}^k a \left( \frac{\nabla u_{h\tau}^i - \nabla u_{h\tau}^{i-1}}{\tau} \right) + \tau C \delta a \left( \frac{\nabla u_{h\tau}^k - \nabla u_{h\tau}^{k-1}}{\tau} \right) + \tau \mu_0 a(\nabla u_{h\tau}^k), \quad (3.22)
\end{aligned}$$

where  $C$  denotes a generic constant which only depends on the problem data, but not on  $h$  and  $\tau$ . We sum this inequality over  $k = 1 \dots N$  for each  $N \leq T/\tau$  and choose  $\delta > 0$  so small that the second and the third term from the last line cancel with terms from the first line. Thus we get

$$\int_{\Omega} \varphi_1(u_{h\tau}^N) + \tau \mu_1 \sum_{k=1}^N a \left( \frac{\nabla u_{h\tau}^k - \nabla u_{h\tau}^{k-1}}{\tau} \right) + \mu_0 a(\nabla u_{h\tau}^N) \leq C + \tau \mu_0 \sum_{k=1}^N a(\nabla u_{h\tau}^k). \quad (3.23)$$

For sufficiently small  $\tau$  the discrete Gronwall inequality shows that  $\sum_{k=1}^N a(\nabla u_{h\tau}^k) \leq C$ . So by (3.23) with  $N = T/\tau$  we have

$$\int_Q a \left( \frac{\partial}{\partial t} \nabla u_{h\tau} \right) \, dx \, dt \leq C, \quad (3.24)$$

and a Poincaré-like inequality gives the desired a priori estimate.  $\square$

**Proposition 3.2** *Each sequence  $\{(u_{h_n, \tau_n}, \omega_{h_n, \tau_n})\}_{n \in \mathbb{N}}$  with  $h_n \rightarrow 0$  and  $\tau_n \rightarrow 0$  has a weakly  $\times$  weakly\* convergent subsequence in  $W^{1,2}(0, T; W_a^{1,2}(\Omega; \mathbb{R}^n)) \times L^\infty(Q; \mathbb{R}^L)$ . The limit of each such subsequence is a weak solution of (2.21). In particular (2.21) has a weak solution.*

*Proof.* We closely follow the proof of [64, Lemma 2], which is inspired by ideas from [16]. By Proposition 3.1 the sequence  $\{(u_{h_n, \tau_n}, \omega_{h_n, \tau_n})\}_{n \in \mathbb{N}}$  is bounded in  $W^{1,2}(0, T; W_a^{1,2}(\Omega; \mathbb{R}^n)) \times L^\infty(Q; \mathbb{R}^L)$ . From Banach's theorem we know that bounded sets in Banach spaces with separable predual are relatively sequentially weakly\* compact, which implies the existence of the subsequence.

In passing to the subsequence, we assume from now on that the sequence converges to a pair  $(u, \omega) \in W^{1,2}(0, T; W_a^{1,2}(\Omega; \mathbb{R}^n)) \times L^\infty(Q; \mathbb{R}^L)$ . Because the imbedding

$$W^{1,2}(0, T; W_a^{1,2}(\Omega; \mathbb{R}^n)) \hookrightarrow L^2(0, T; W^{1,2}(\Omega; \mathbb{R}^n))$$

is compact,  $u_{h_n, \tau_n}$  converges strongly to  $u$  in  $L^2(0, T; W^{1,2}(\Omega; \mathbb{R}^n))$ . Since  $\|\nabla \bar{u}_{h_n, \tau_n} - \nabla u_{h_n, \tau_n}\|_{L^2(Q; \mathbb{R}^{n \times n})} = \mathcal{O}(\tau)$  due to the a priori estimate (3.21) we also have  $\bar{u}_{h_n, \tau_n} \rightarrow u$  strongly in  $L^2(0, T; W^{1,2}(\Omega; \mathbb{R}^n))$ . From (3.6) we infer that the discrete solution satisfies

$$\begin{aligned}
&\int_0^T \int_{\Omega} \left( \sum_{\ell \in L} \bar{\omega}_{h_n, \tau_n, \ell} \lambda'_\ell(\nabla \bar{u}_{h_n, \tau_n}) + \sigma(\nabla \bar{u}_{h_n, \tau_n}) \right) : \nabla v_{h_n} - \bar{f}_{h_n, \tau_n} \cdot v_{h_n} \, dx \\
&\quad - \int_{\Gamma_1} \bar{g}_{h_n, \tau_n} \cdot v_{h_n} \, dS + \left\langle \sigma_a \left( \mu_1 \frac{\partial}{\partial t} \nabla u_{h_n, \tau_n} + \mu_0 \nabla \bar{u}_{h_n, \tau_n} \right), \nabla v_{h_n} \right\rangle \, dt = 0 \quad (3.26)
\end{aligned}$$

for all  $v_{h_n} \in V_{h_n}$ . We have weak convergence for the linear terms and strong convergence for the nonlinear terms and thus we directly obtain (2.23a) for all  $v \in \bigcup_n V_{h_n}$  and therefore for all  $v \in V$  by density.

From (3.7) it follows that

$$\int_0^T \int_{\Omega} (\bar{\omega}_{h_n, \tau_n, \ell} - z_{h_n}) \left( \frac{\partial}{\partial t} [\lambda_\ell(\nabla u_{h_n, \tau_n})]_\tau - v_{h_n} \right) \geq 0 \quad (3.27)$$

for all  $v_{h_n} \in V_{h_n}$  and all  $z_{h_n} \in L_{h_n}$  with  $z_{h_n} \in \text{sign } v_{h_n}$ . Here, for a piecewise constant function  $\bar{v}$ , the term  $[\bar{v}]_\tau$  denotes the piecewise affine interpolation such that  $[\bar{v}]_\tau(k\tau) = \bar{v}|_{((k-1)\tau, k\tau)}$ . We use (3.26) and (2.23a) to circumvent the limit process of the product of two weakly or weakly\*, respectively, convergent functions:

$$\begin{aligned}
& \limsup_{n \rightarrow \infty} \int_Q \sum_{\ell \in L} \bar{\omega}_{h_n \tau_n, \ell} \frac{\partial}{\partial t} [\lambda_\ell(\nabla u_{h_n \tau_n})]_\tau \\
& \leq \limsup_{n \rightarrow \infty} \int_Q \sum_{\ell \in L} \bar{\omega}_{h_n \tau_n, \ell} \lambda'_\ell(\nabla \bar{u}_{h_n \tau_n}) : \frac{\partial}{\partial t} \nabla u_{h_n \tau_n} + C\tau_n \\
& = \limsup_{n \rightarrow \infty} - \int_Q \sigma(\nabla \bar{u}_{h_n \tau_n}) : \frac{\partial}{\partial t} \nabla u_{h_n \tau_n} + \int_Q \bar{f}_{\tau_n} \cdot \frac{\partial}{\partial t} u_{h_n \tau_n} + \int_{\Gamma_1} \bar{g}_{\tau_n} \cdot \frac{\partial}{\partial t} u_{h_n \tau_n} \\
& \quad - \int_0^T \left\langle \sigma_a \left( \mu_1 \frac{\partial}{\partial t} \nabla u_{h_n \tau_n} + \mu_0 \nabla \bar{u}_{h_n \tau_n} \right), \frac{\partial}{\partial t} \nabla u_{h_n \tau_n} \right\rangle \\
& \leq \limsup_{n \rightarrow \infty} - \int_Q \sigma(\nabla \bar{u}_{h_n \tau_n}) : \frac{\partial}{\partial t} \nabla u_{h_n \tau_n} + \int_Q \bar{f}_{\tau_n} \cdot \frac{\partial}{\partial t} u_{h_n \tau_n} + \int_{\Gamma_1} \bar{g}_{\tau_n} \cdot \frac{\partial}{\partial t} u_{h_n \tau_n} \\
& \quad - 2\mu_1 \int_0^T a \left( \frac{\partial}{\partial t} \nabla u_{h_n \tau_n} \right) dt - \mu_0 a(\nabla u_{h_n \tau_n}(\cdot, T)) + \mu_0 a(\nabla u_0) \\
& \leq - \int_Q \sigma(\nabla u) : \frac{\partial}{\partial t} \nabla u + \int_Q f \cdot \frac{\partial}{\partial t} u + \int_{\Gamma_1} g \cdot \frac{\partial}{\partial t} u - 2\mu_1 \int_0^T a \left( \frac{\partial}{\partial t} \nabla u \right) dt \\
& \quad - \mu_0 a(\nabla u(\cdot, T)) + \mu_0 a(\nabla u_0) \\
& = \int_Q \sum_{\ell \in L} \omega_\ell \lambda'_\ell(\nabla u) : \frac{\partial}{\partial t} \nabla u. \tag{3.28}
\end{aligned}$$

Here we used the weak upper semicontinuity of the quadratic form  $-a$ . By an appropriate choice of the test functions we pass from the sum over all  $\ell$  to the single inequalities for each  $\ell$  and finally obtain (2.23b).  $\square$

#### 4 Computational experiments

In the following we apply our model to the cubic to tetragonal transformation in an Indium-Thallium alloy and present computational experiments for various loading regimes. In Sect. 4.1 and 4.2 we give the material data and the geometric description of the considered problems. Then, in Sect. 4.3 we discuss the results of our numerical experiments.

##### 4.1 Material data

The material properties of shape memory alloys are described by the associated stored energy density  $\varphi : \mathbb{R}^{3 \times 3} \rightarrow \mathbb{R}$ . However, even though up to now already a lot of different materials have been examined both theoretically and experimentally, the detailed form of the associated  $\varphi$  can in general not be found in the literature. A certain exception is the cubic to tetragonal transformation of In-20.7 at% Tl alloy. Here, Ericksen and James [21, 22] (see also [17, 45, 49]) used the potential  $\varphi$  (dependent on temperature  $\vartheta$ ) in the form

$$\begin{aligned}
\varphi_\vartheta(F) &= \frac{a(\vartheta)}{6} \left[ \left( \frac{3C_{11}}{\text{tr } C} - 1 \right)^2 + \left( \frac{3C_{22}}{\text{tr } C} - 1 \right)^2 + \left( \frac{3C_{33}}{\text{tr } C} - 1 \right)^2 \right] \\
& \quad + \frac{b}{2} \left( \frac{3C_{11}}{\text{tr } C} - 1 \right) \left( \frac{3C_{22}}{\text{tr } C} - 1 \right) \left( \frac{3C_{33}}{\text{tr } C} - 1 \right) \\
& \quad + \frac{c}{36} \left[ \left( \frac{3C_{11}}{\text{tr } C} - 1 \right)^2 + \left( \frac{3C_{22}}{\text{tr } C} - 1 \right)^2 + \left( \frac{3C_{33}}{\text{tr } C} - 1 \right)^2 \right]^2 \\
& \quad + \frac{d}{2} (C_{12}^2 + C_{13}^2 + C_{23}^2 + C_{21}^2 + C_{31}^2 + C_{32}^2) + e(\text{tr } C - 3)^2 \tag{4.1}
\end{aligned}$$

with  $C = F^T F$  and  $\text{tr } C = C_{11} + C_{22} + C_{33}$ . The material constants are  $a(\vartheta) = 0.38 + (1.22 \times 10^{-3})(\vartheta - \vartheta_T)$ ,  $b = -29.23$ ,  $c = 562.13$ ,  $d = 3.26$ ,  $e = 5.25$ , (all in GPa) and  $\vartheta_T = 70^\circ\text{C}$ . This potential is obviously frame indifferent in the sense that  $\varphi_\vartheta(RF) = \varphi_\vartheta(F)$  holds for all  $R \in \text{SO}(3)$ . Its growth as polynomial of degree four does not fit our data qualification (2.24a). But in our calculations the deformation gradients were always small and bounded, and the energy density was mostly designed to reflect the material properties for small deformation gradients. Hence  $\varphi_\vartheta(F)$  can be modified for large  $F$  such that it grows quadratically as  $|F| \rightarrow +\infty$ , and (2.24a) is fulfilled.

The local minima of  $\varphi_\vartheta$  are attained at four wells  $\text{SO}(3)U_\alpha$ :

$$\begin{aligned} U_1 &= \text{diag}(\eta_2, \eta_1, \eta_1), & (\text{martensite - tetragonal, variant 1}) , \\ U_2 &= \text{diag}(\eta_1, \eta_2, \eta_1), & (\text{martensite - tetragonal, variant 2}) , \\ U_3 &= \text{diag}(\eta_1, \eta_1, \eta_2), & (\text{martensite - tetragonal, variant 3}) , \\ U_4 &= \text{I} = \text{diag}(1, 1, 1) & (\text{austenite - cubic}) , \end{aligned} \quad (4.2)$$

where  $\eta_1 < 1$  and  $\eta_2 > 1$ . Both parameters depend on the temperature. They are given in [21] as

$$\eta_1(\vartheta) = \sqrt{1 - \epsilon(\vartheta)}, \quad \eta_2(\vartheta) = \sqrt{1 + 2\epsilon(\vartheta)}, \quad \epsilon(\vartheta) = \frac{-3b + \sqrt{9b^2 - 32a(\vartheta)c}}{8c}. \quad (4.3)$$

The energies of the wells are mutually equal at the temperature  $\vartheta = 108.92^\circ\text{C}$ , i.e. austenite is in equilibrium with martensite. If  $\vartheta < 108.92^\circ\text{C}$ , martensite dominates, i.e. it has a lower energy than austenite, and vice versa for  $\vartheta > 108.92^\circ\text{C}$ . In the following experiments we fix the temperature to  $\vartheta = 20^\circ\text{C}$ . Consequently the martensite phase is dominant and  $\epsilon(\vartheta) \doteq 0.0293$ .

Next, we design the plastic dissipative mechanism in accordance with Sect. 2. To match the simulation results to the results of real experiments it would be necessary to identify the transformation energies  $\mathcal{E}_{\alpha\beta}$  for each pair  $(\alpha, \beta)$ . Unfortunately we do not have them at our disposal, so we assume that they are all equal. For this it suffices to consider  $L = \{\{1\}, \{2\}, \{3\}, \{4\}\}$  only. Each  $\lambda_\ell$  is zero in a neighbourhood of the well  $U_\alpha$  with  $\ell = \{\alpha\}$  and takes the value  $\Lambda \geq 0$  in a neighbourhood of the other wells. The decisive criterion for the distance is the Frobenius norm  $\|C\|_F = \left(\sum_{i,j} c_{ij}^2\right)^{1/2}$  of the Cauchy-Green strain tensor  $C = F^T F$ . Away from the wells we interpolate with a polynomial to achieve a smooth function. Altogether we use

$$\lambda_\ell(F) = \Lambda \cdot \begin{cases} 0 & \text{if } d_\ell(F^T F) \leq -\varepsilon_\ell, \\ 1 & \text{if } d_\ell(F^T F) \geq \varepsilon_\ell, \\ \frac{1}{2} + \frac{3}{4} \frac{d_\ell(F^T F)}{\varepsilon_\ell} - \frac{1}{4} \left(\frac{d_\ell(F^T F)}{\varepsilon_\ell}\right)^3 & \text{otherwise} \end{cases} \quad (4.4)$$

with

$$d_\ell(C) = \|C - U_\ell^T U_\ell\|_F^2 - \min_{\alpha \neq \ell} \|C - U_\alpha^T U_\alpha\|_F^2. \quad (4.5)$$

Here, the parameter

$$\varepsilon_\ell = \frac{1}{2} \min_{\alpha \neq \ell} \|U_\ell^T U_\ell - U_\alpha^T U_\alpha\|_F^2 \quad (4.6)$$

describes a suitable tolerance.<sup>3</sup> The decision function  $d_\ell(C)$  is negative if and only if the Cauchy-Green strain  $C$  is closer to the well  $\ell$  than to any other well. In view of (2.3), the mechanism (4.4)–(4.5) for  $\alpha \neq \beta$  results in

$$\mathcal{E}_{\alpha\beta} = \sum_{\ell=1}^4 |\lambda_\ell(U_\alpha) - \lambda_\ell(U_\beta)| = \Lambda + \Lambda + 0 + 0 = 2\Lambda, \quad (4.7)$$

<sup>3</sup> The non-differentiable function “min” may be smoothed by replacing it with  $\min^\varepsilon(a_1, a_2, a_3) = \varepsilon \ln(e^{-a_1/\varepsilon} + e^{-a_2/\varepsilon} + e^{-a_3/\varepsilon})$ , where  $\varepsilon > 0$ . Nevertheless this turned out to be unnecessary for our numerical experiments.



independent of  $\alpha$  and  $\beta$ . Values of  $\Lambda$  of about  $1 \text{ MJm}^{-3}$  turned out to be reasonable.

The coefficient  $\mu_0$  reflects the interfacial stored energy. It is indeed observed that finely twinned martensites have higher energies than single-phase regions. In such a manner,  $\mu_0$  could be fitted to the result of an experiment if available. Here, however, we use  $\mu_0 = 0$ .

For the definition of  $\gamma$  and  $\mu_1$  we do not have any hint from experiments. We choose  $\gamma = 0.25$  and  $\mu_1 = 10 \text{ GPa m}^{2\gamma}\text{s}$  for the tensile experiment and  $\mu_1 = 100 \text{ GPa m}^{2\gamma}\text{s}$  for the shear experiment. By this choice the influence of the viscous term under the given loading regimes does not destroy the stored energy and the rate-independent dissipation mechanisms which are essential for the hysteretic response we want to simulate. On the other hand,  $\mu_1$  is large enough that the regularizing effect of the viscous term appears. In comparison to the case  $\mu_1 = 0$  (for which the theoretical justification of the calculations is unclear), we observed a smaller error in the a posteriori energy balance.

#### 4.2 Geometric data and loading regimes

Let us first remark that the capillarity and viscosity terms determine the length scale of the occurring microstructure but, beyond that, the length scale of the specimen is not determined by the model. Therefore it makes no sense to describe the dimensions of the specimen in our numerical experiments in concrete physical units. Instead we work with dimensionless numbers for the lengths. In the following, let the domain  $\Omega$  be the unit cube  $(-\frac{1}{2}, \frac{1}{2})^3$ . In consistence with common laboratory experiments, we neglect the body forces and the surface pressure, i.e.  $f = 0$  and  $g = 0$ . The hard-device loading<sup>4</sup> is achieved by controlling the deformation  $u_D$  on two opposite faces of the cube  $\Omega$ , namely  $\Gamma_0 = \{(-\frac{1}{2}, x_2, x_3) \in \partial\Omega\} \cup \{(\frac{1}{2}, x_2, x_3) \in \partial\Omega\}$ . This corresponds to a  $(1, 0, 0)$ -orientation of the crystal. Two different regimes were tested: tensile and shear loading, cf. Fig. 4.1.

To be more specific, we use

$$u_D(t, -\frac{1}{2}, x_2, x_3) = \left(-\frac{1}{2} + s(t), x_2, x_3\right), \quad u_D(t, \frac{1}{2}, x_2, x_3) = \left(\frac{1}{2} - s(t), x_2, x_3\right) \quad (4.8)$$

for the tensile loading experiments (starting with compression) and

$$u_D(t, -\frac{1}{2}, x_2, x_3) = \left(-\frac{1}{2}, x_2 + s(t), x_3\right), \quad u_D(t, \frac{1}{2}, x_2, x_3) = \left(\frac{1}{2}, x_2 - s(t), x_3\right) \quad (4.9)$$

for the shear loading experiments. The periodic cycling was implemented by a function  $s(t)$  with sawtooth form and amplitude  $A$  as shown in Fig. 4.2. Note that this load  $u_D$  satisfies the smoothness condition (2.24c).

In all experiments the crystal lattice is oriented parallel to the coordinate axes. The starting value  $u^0$  is the randomly disturbed identity mapping.

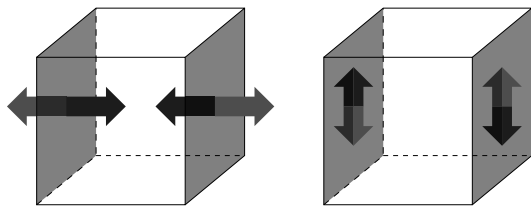


**Fig. 4.1.** Schematic illustration of hard-device loading conditions  $u_D$ : tensile and shear loading

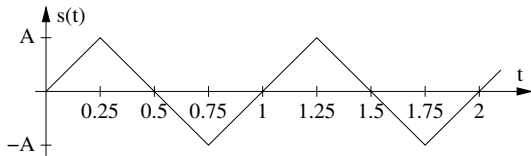


**Fig. 4.2.** The periodically cycling  $s = s(t)$

<sup>4</sup> Let us remark that in laboratory experiments hard loading device boundary conditions are just as difficult to achieve as purely load controlled experiments due to the relatively low stiffness of every loading device.

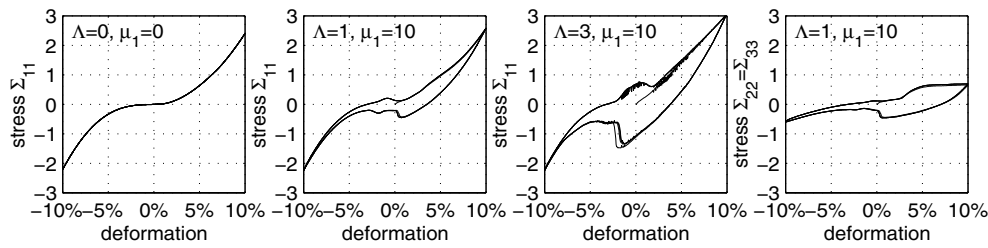


Fig. 4.3. Stress/deformation diagram for the tensile loading experiment.  $\Sigma$  in GPa,  $\Lambda$  in  $\text{MJm}^{-3}$ ,  $\mu_1$  in  $\text{GPa m}^{2\gamma_s}$

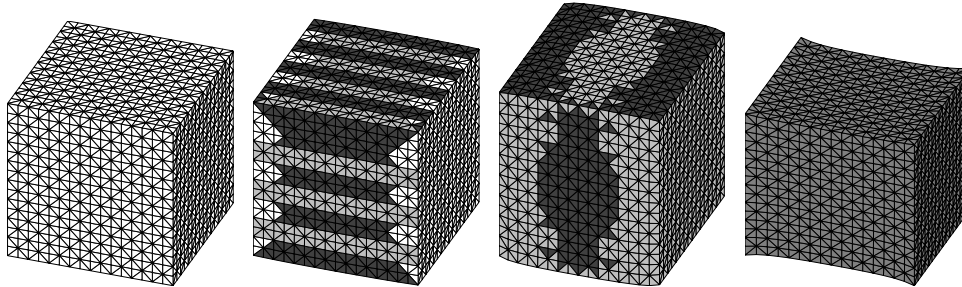


Fig. 4.4. Deformed specimen for tensile loading experiment at times  $t = 0$ ,  $t = 0.0375$ ,  $t = 0.25$  and  $t = 0.75$  for  $\Lambda = 0$

### 4.3 Responses on various loading regimes

The results of our computational experiments are, like the results from laboratory experiments, quite complex and it is not easy to select and display the most representative features. In the following we display averaged stress/deformation diagrams for different values of  $\Lambda$ , the time evolution of volume fractions of certain phases, the relative error in the energy balance and some snapshots of the InTi specimen under loading. For all experiments we fix the mesh size  $h$  in the space discretization to  $h = 1/16$  and the time step size to  $\tau = 1/800$ , i.e. 800 steps per loading cycle.

*Tensile Loading Experiment:* First, we present the results for the tensile loading case. The experimentally most wanted output are the stress/deformation diagrams. To demonstrate the influence of the parameter  $\Lambda$  (see (4.5)–(4.7)) we consider two values  $\Lambda = 3 \text{ MJm}^{-3}$  and  $\Lambda = 1 \text{ MJm}^{-3}$ . For comparison we performed the calculations also for  $\Lambda = 0 \text{ MJm}^{-3}$ , i.e. without plastic-like dissipation. There are nine possible diagrams, each displays one component of the  $3 \times 3$ -tensor  $\Sigma := \int_{\Omega} \sigma(\nabla u) dx$ . In Fig. 4.3 we present the  $x_1$ -component of the stress in  $x_1$ -direction for different values of  $\Lambda$ . We see that the size of  $\Lambda$  clearly influences the hysteresis behaviour of the process. While for  $\Lambda = 0$  there is naturally no hysteresis effect to be expected, we clearly obtain for  $\Lambda = 1 \text{ MJm}^{-3}$  a hysteresis loop. For unphysically large values of  $\Lambda$  such as  $\Lambda = 3 \text{ MJm}^{-3}$  the hysteresis loop of course increases, but shows unnatural effects. The  $\Sigma_{22}$ -component is also displayed. The results for the  $\Sigma_{33}$ -component were analogous to that for the  $\Sigma_{22}$ -component. The remaining six stress components are nearly zero. Note that the area of the hysteresis loop in the  $\Sigma_{11}$  diagram corresponds to the amount of the dissipated energy spent for all phase transformations and for viscous damping, see the energy balance (2.28).

To get an impression of the evolution in time, we present the deformed specimen at four different time steps. The austenite phase is indicated in white, the martensite phases are indicated in different gray shades.

An interesting information, usually not available in laboratory experiments, is the time evolution of the volume fractions of the particular phases. We present it in Fig. 4.5 for  $\Lambda = 3 \text{ MJm}^{-3}$ . The phase fraction diagrams give a good hint about qualitative properties of the specimen. For the tensile loading experiment, we see from Fig. 4.5 that the austenite phase is dominant around  $t = 1, 2, 3, \dots$  (not  $t = 0$  because of the random starting value), compare with the first cube in Fig. 4.4. Then around  $t = 0.1 \dots 0.4$ ,  $t = 1.1 \dots 1.4, \dots$  the phase fraction diagram indicates mainly an approximately equal mixture of two martensite phases, which appears in form of different microstructures, compare the second and third cube. Finally around  $t = 0.6 \dots 0.9$ ,  $t = 1.6 \dots 1.9, \dots$  the phase fractions indicate a mostly pure third austenite phase, see the fourth cube. We can illustrate this by the

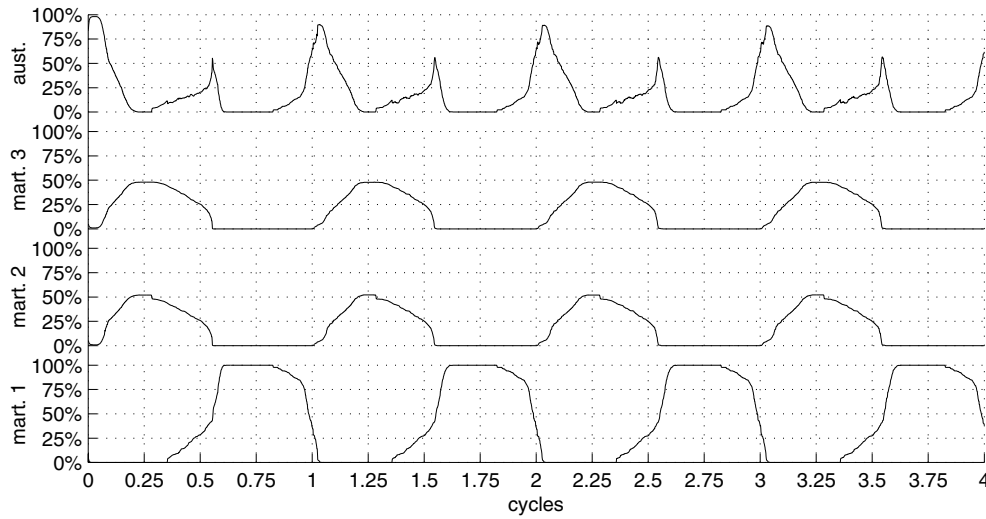


Fig. 4.5. Phase fractions for tensile loading experiment for  $\Lambda = 3 \text{ MJm}^{-3}$ ,  $\mu_0 = 0 \text{ GPa m}^{2\gamma}$ ,  $\mu_1 = 10 \text{ GPa m}^{2\gamma}\text{s}$

diagram



A direct martensite–martensite transformation almost never occurs, instead we observe martensite–austenite transformations only.

Note that in the numerical simulation the energy balance (2.28) only needs to be satisfied approximately. To check it we relate its numerical error to the total amount of energy exchanged in the system. This gives an interesting a posteriori information about the discretization error and the quality of the minimization procedure solving (3.9). To be precise, the relative error at time  $k$  is defined by

$$E_{\text{rel}}^k = \left| \frac{E^k - E^0 + D^k + V^k - W^k}{E^k - E^0 + D^k + V^k + W_{\text{abs}}^k} \right| \quad (4.11)$$

with

$$\begin{aligned}
 E^k &= \int_{\Omega} \varphi(\nabla u_{h\tau}^k) \, dx + \mu_0 a(\nabla u_{h\tau}^k), & \text{(stored energy) ,} \\
 D^k &= \sum_{t=1}^k \sum_{\ell \in L} \int_{\Omega} |\lambda_{\ell}(\nabla u_{h\tau}^t) - \lambda_{\ell}(\nabla u_{h\tau}^{t-1})| \, dx, & \text{(dissipation) ,} \\
 V^k &= 2\mu_1 \sum_{t=1}^k a\left(\frac{\nabla u_{h\tau}^t - \nabla u_{h\tau}^{t-1}}{\tau}\right), & \text{(viscosity) ,} \\
 W^k &= \sum_{t=1}^k \langle \sigma_{\nu}(\nabla u_{h\tau}^k), u_{h\tau}^t - u_{h\tau}^{t-1} \rangle, & \text{(external work) ,} \\
 W_{\text{abs}}^k &= \sum_{t=1}^k |\langle \sigma_{\nu}(\nabla u_{h\tau}^k), u_{h\tau}^t - u_{h\tau}^{t-1} \rangle|, & \text{(absolute external work) .}
 \end{aligned}
 \quad (4.12)$$

The relative error in the energy balance is displayed in Fig. 4.6. As expected, a higher contribution of the dissipative mechanism introduces an additional error in the balance. Nevertheless, even for  $\Lambda = 3 \text{ MJm}^{-3}$  the relative error is only about 1% which is quite acceptable.

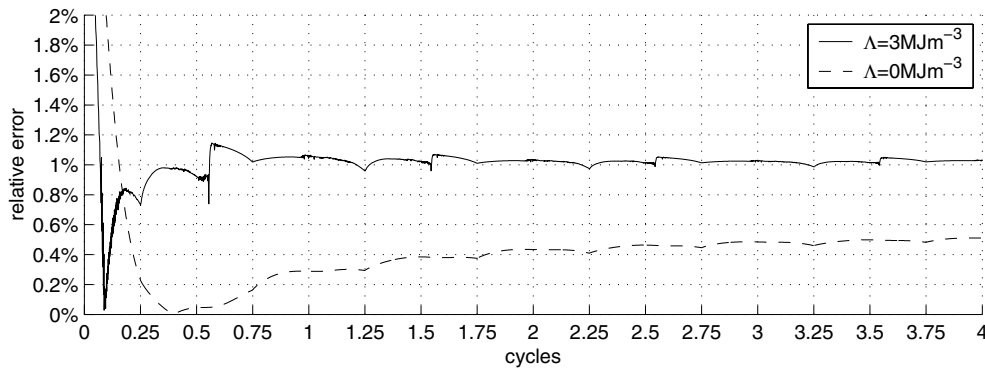


**Fig. 4.6.** Relative error in the energy balance for the tensile loading experiment with  $\mu_0 = 0 \text{ GPa m}^{2\gamma\text{s}}$ ,  $\mu_1 = 10 \text{ GPa m}^{2\gamma\text{s}}$ ,  $\Lambda = 3 \text{ MJm}^{-3}$  (bold line) and  $\Lambda = 0 \text{ MJm}^{-3}$  (dashed line)

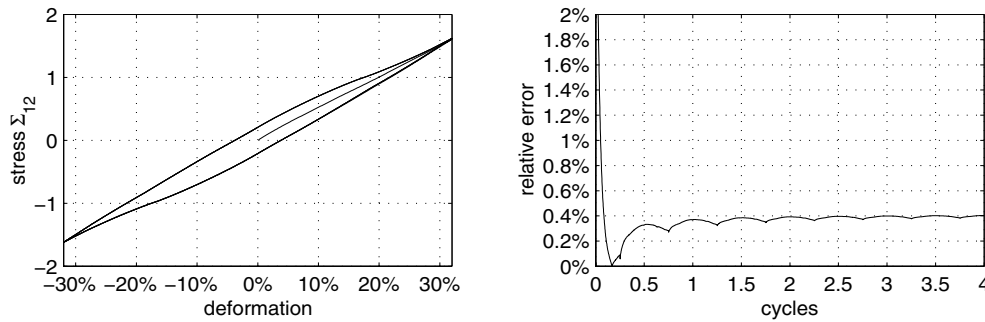


**Fig. 4.7.** Stress/deformation diagram for  $\Sigma_{12}$ , energy balance for shear experiment,  $\Lambda = 3 \text{ MJm}^{-3}$ ,  $\mu_0 = 0 \text{ GPa m}^{2\gamma}$ ,  $\mu_1 = 100 \text{ GPa m}^{2\gamma\text{s}}$

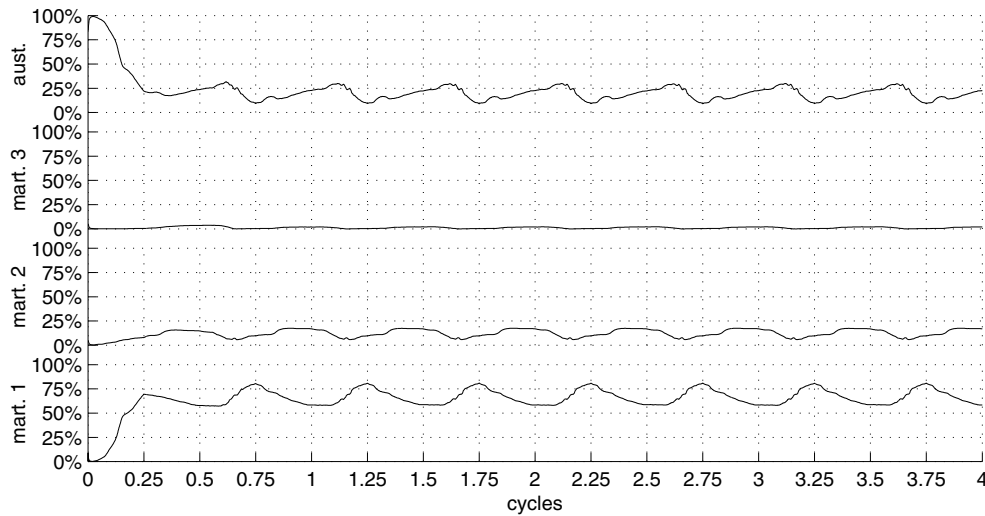


**Fig. 4.8.** Phase fractions for shear experiment,  $\Lambda = 1 \text{ MJm}^{-3}$ ,  $\mu_0 = 0 \text{ GPa m}^{2\gamma}$ ,  $\mu_1 = 100 \text{ GPa m}^{2\gamma\text{s}}$

*Shear Loading Experiment:* We now briefly present the results for the shear loading case. In Fig. 4.7 (left) we give the stress/deformation diagram of  $\Sigma_{12}$  for  $\Lambda = 3 \text{ MJm}^{-3}$ . Again we observe a substantial hysteresis effect. The corresponding relative error in the energy balance is given in Fig. 4.7 (right). It stays well below 0.4%.

The phase fraction diagram for this experiment with  $\Lambda = 1 \text{ MJm}^{-3}$  is shown in Fig. 4.8. Note that the cycles of phases are not aligned with these of the boundary values, but are a little bit delayed. This effect is introduced by the dissipative mechanism, which remembers to some extent the previous configuration. The phase fraction diagram reveals that the martensitic phases M2 and M3 are mostly not present. The corresponding transformation

process can be described by the diagram



Note that we again observe only martensite–austenite transformations and no direct martensite–martensite transformations.

## 5 Concluding remarks

Based on [64,65,71], we developed a continuum-mechanical model for isothermal laboratory experiments of single-crystal shape-memory alloys. Beside capillarity- and viscosity-like terms it involves a phenomenological rate-independent dissipation mechanism which incorporates the energy dissipation of phase transformations. We discretized the model with finite elements and applied wavelet techniques for the higher order terms. Supported by a convergence analysis, we performed three-dimensional numerical experiments for an InTi single-crystal under hard-device loading.

The numerical experiments indicate that the model is capable to simulate the behaviour of martensitic transformations in shape-memory alloys. This sort of calculations can complement laboratory experiments by data which is otherwise hardly or not at all accessible, like for example the volume fractions or stresses inside the specimen. To some extent, it seems possible to run simulations for experiments which cannot be performed in real laboratories and to predict the behaviour of new materials.

*Acknowledgements.* This research was pursued during T.R.'s stay at the University of Bonn. The support from the SFB 256 and partly also from the grants 201/00/0768 (GA ČR), A 107 5005 (GA AV ČR) and MSM 11320007 (MŠMT ČR) is gratefully acknowledged. The authors are also thankful to V. Novák and P. Šittner for valuable comments.

## References

1. Abeyaratne, R., Knowles, J.K.: Implications of viscosity and strain-gradient effects for the kinetics of propagating phase boundaries in solids. *SIAM J. Appl. Math.* **51**, 1205–1221 (1991)
2. Abeyaratne, R., Chu, C., James, R.D.: Kinetics of materials with wiggly energies: theory and application to the evolution of twinning microstructures in a Cu–Al–Ni shape memory alloy. *Phil. Mag. A* **73**, 457–497 (1996)
3. Alberti, G., Müller, S.: A new approach to variational problems with multiple scales. *Commun. Pure Appl. Math.* **54**, 761–825 (2001)
4. Alt, H.W., Hoffmann, K.H., Niezgodka, M., Sprekels, J.: A numerical study of structural phase transitions in shape memory alloys. Preprint no. 90, Math. Institut, Universität Augsburg (1985)
5. Andrews, G.: On the existence of solutions to the equation  $u_{tt} = u_{xxt} + \sigma(u_x)_x$ . *J. Differ. Equations* **35**, 200–231 (1980)
6. Ball, J.M., Holmes, P.J., James, R.D., Pego, R.L., Swart, P.J.: On the dynamics of fine structure. *J. Nonlinear Sci.* **1**, 17–70 (1991)
7. Ball, J.M., James, R.D.: Fine phase mixtures as minimizers of energy. *Arch. Ration. Mech. Anal.* **100**, 13–52 (1987)
8. Ball, J.M., James, R.D.: Proposed experimental tests of a theory of fine microstructure and the two-well problem. *Phil. Trans. R. Soc. Lond. Ser. A* **338**, 389–450 (1992)
9. Bhattacharya, K., Firoozye, N.B., James, R.D., Kohn, R.V.: Restrictions on microstructure. *Proc. R. Soc. Edinb. Sect. A* **124**, 843–878 (1994)
10. Brandt, A., Sandak, B.: Multilevel summation methods for N-body interactions. In: Brandt, A., Bernholc, J., Binder, K. (eds): *Multiscale Computational Methods in Chemistry and Physics*. Amsterdam: NATO Science Series, IOS Press, pp. 3–31 (2001)
11. Brandt, A., Venner, C.H.: Multilevel evaluation of integral transforms with asymptotically smooth kernels. *SIAM J. Sci. Comput.* **19**, 468–492 (1998)
12. Brokate, M., Sprekels, J.: *Hysteresis and Phase Transitions*. New York: Springer (1996)
13. Bubner, N.: Landau-Ginzburg model for a deformation-driven experiment on shape memory alloys. *Contin. Mech. Thermodyn.* **8**, 293–308 (1996)
14. Carstensen, C., Dolzmann, G.: Time-space discretization of the nonlinear hyperbolic system  $u_{tt} = \operatorname{div}(\sigma(Du) + Du_t)$ . Preprint No. 60/2001, Max-Planck-Institut Leipzig (2001)
15. Clarke, F.H.: *Optimization and Nonsmooth Analysis*. New York: Wiley (1983)
16. Colli, P., Visintin, A.: On a class of doubly nonlinear evolution equations. *Commun. Partial Differ. Equations* **15**, 737–756 (1990)

17. Collins, C., Luskin, M.: The computation of the austenitic-martensitic phase transition. In: Rascle, M., Serre, D., Slemrod, M. (eds): PDEs and Cont. Models of Phase Transitions. Lecture Notes in Physics 344. New York: Springer, pp. 34–50 (1989)
18. Dafermos, C.M.: The mixed initial-boundary value problems for equation of nonlinear one-dimensional viscoelasticity. *J. Differ. Equations* **6**, 71–86 (1969)
19. Dahmen, W., Stevenson, R.: Element-by-element construction of wavelets satisfying stability and moment conditions. *SIAM J. Numer. Anal.* **37**, 319–352 (1999)
20. Eve, R.A., Reddy, B.D., Rockafellar, R.T.: An internal variable theory of elastoplasticity based on the maximum plastic work inequality. *Q. Appl. Math.* **48**, 59–83 (1990)
21. Ericksen, J.: Constitutive theory for some constrained elastic crystals. *Int. J. Solids Struct.* **22**, 951–964 (1986)
22. Ericksen, J.: Some constrained elastic crystals. In: Ball J (ed) *Material Instabilities in Continuum Mechanics and Related Problems*. Oxford: Oxford Univ. Press, pp. 119–137 (1987)
23. Falk, F.: Model free energy, mechanics and thermodynamics of shape memory alloys. *Acta Metallurgica* **28**, 1773–1780 (1980)
24. Falk, F., Konopka, P.: Three-dimensional Landau theory describing the martensitic phase transformation of shape-memory alloys. *J. Condens. Matter* **2**, 61–77 (1990)
25. Frémond, M.: Matériaux à mémoire de forme. *C.R. Acad. Sci. Paris* 304, Série II, 239–244 (1987)
26. Frémond, M., Miyazaki, S.: *Shape memory alloys*. Wien: Springer (1996)
27. Friesecke, G., Dolzmann, G.: Implicit time discretization and global existence for a quasi-linear evolution equation with nonconvex energy. *SIAM J. Math. Anal.* **28**, 363–380 (1997)
28. Garcke, H.: Travelling wave solutions as dynamic phase transitions in shape memory alloys. *J. Differ. Equations* **121**, 203–231 (1995)
29. Gill, P.E., Murray, W.: *Numerical methods for constrained optimization*. London: Academic Press (1974)
30. Gimbutas, Z., Greengard, L., Minion, M.: Coulomb interactions on planar structures: inverting the square root of the Laplacian. *SIAM J. Sci. Comput.* **22**, 2093–2108 (2001)
31. Greengard, L., Rokhlin, V.: A fast algorithm for particle simulations. *J. Comp. Physics* **73**, 325–348 (1987)
32. Greengard, L., Rokhlin, V.: A new version of the fast multipole method for the Laplace equation in three dimensions. *Acta Numer.* **6**, 229–269 (1997)
33. Griebel, M., Oswald, P.: Tensor product type subspace splitting and multilevel iterative methods for anisotropic problems. *Adv. Comput. Math.* **4**, 171–206 (1995)
34. Hackbusch, W.: A sparse matrix arithmetic based on  $\mathcal{H}$ -matrices. Part I: Introduction to  $\mathcal{H}$ -matrices. *Computing* **62**, 89–108 (1999)
35. Hackbusch, W., Nowak, Z.P.: On the fast matrix multiplication in the boundary element method by panel clustering. *Numer. Math.* **54**, 463–491 (1989)
36. Hernquist, L.: Performance characteristics of tree codes. *Astrophys. J. Suppl. Ser.* **64**, 715–734 (1987)
37. Hill, R.: A variational principle of maximum plastic work in classical plasticity. *Q. J. Mech. Appl. Math.* **1**, 18–28 (1948)
38. Hoffmann, K.H., Zochowski, A.: Existence of solutions to some non-linear thermoelastic systems with viscosity. *Math. Methods Appl. Sci.* **15**, 187–204 (1992)
39. Huo, Y., Müller, I.: Nonequilibrium thermodynamics of pseudoelasticity. *Contin. Mech. Thermodyn.* **5**, 163–204 (1993)
40. Huo, Y., Müller, I., Seelecke, S.: Quasiplasticity and pseudoelasticity in shape memory alloys. In: Brokate, M. et al. (eds): *Phase Transitions and Hysteresis*. Lecture Notes in Math. 1584. Berlin: Springer, pp. 87–146 (1994)
41. Idesman, A.V., Levitas, V.I., Stein, E.: Elastoplastic materials with martensitic phase transition and twinning at finite strains: numerical solution with the finite element method. *Comput. Methods Appl. Mech. Eng.* **173**, 71–98 (1999)
42. James, R.D.: Hysteresis in phase transformations. In: Kirchgaessner K et al (eds) *ICIAM 95, Proc. 3rd Int. Congress Indust. Appl. Math.* Akademie Verlag, Berlin, Math. Res. 87, pp 135–154 (1996)
43. Johnson, C.: On Plasticity with Hardening. *J. Math. Anal. Appl.* **62**, 325–336 (1978)
44. Klouček, P., Luskin, M.: The computation of the dynamics of the martensitic transformation. *Continuum Mech. Thermodyn.* **6**, 209–240 (1994)
45. Klouček, P., Luskin, M.: Computational modeling of the martensitic transformation with surface energy. *Math. Comp. Modelling* **20**, 101–121 (1994)
46. Koster, F.: *Multiskalen-basierte Finite Differenzen Verfahren auf adaptiven dünnen Gittern*. Dissertation, Institute for Applied Mathematics, University of Bonn (2002)
47. Leclerq, S., Bourbon, G., LExcellent, C.: Plasticity like model of martensite phase transition in shape memory alloys. *J. Physique III* **5**, 513–518 (1995)
48. Luenberger, D.: *Optimization by vector space methods*. New York: Wiley (1969)
49. Luskin, M.: On the computation of crystalline microstructure. *Acta Numer.* **5**, 191–257 (1996)
50. Mandel, J.: Energie élastique et travail dissipé dans les modèles. *Cahiers Groupe Français de Rhéologie* **1**, 9–13 (1965)
51. Maugin, G.A.: *The thermomechanics of plasticity and fracture*. Cambridge: Cambridge Univ. Press (1992)
52. Mielke, A., Theil, F., Levitas, V.I.: A variational formulation of rate-independent phase transformations using an extremum principle. *Arch. Ration. Mech. Anal.* **162**, 137–177 (2002)
53. Müller, I.: On the size of the hysteresis in pseudoelasticity. *Contin. Mech. Thermodyn.* **1**, 125–142 (1989)
54. Müller, I., Seelecke, S.: Thermodynamic aspects of shape memory alloys. *Math. Comput. Modelling* **34**, 1307–1355 (2001)
55. Müller, I., Xu, H.: On the pseudo-elastic hysteresis. *Acta Metallurgica et Mater.* **39**, 263–271 (1991)
56. Müller, S.: Singular perturbations as a selection criterion for periodic minimizing sequences. *Calc. Var. Partial Differ. Equ.* **1**, 169–204 (1993)
57. Müller, S.: Variational models for microstructure and phase transitions. *Lecture Notes No. 2*, Max-Planck-Institut Leipzig (1998)

58. Niezgodka, M., Sprekels, J.: Existence of solutions for a mathematical model of structural phase transitions in shape memory alloys. *Math. Methods Appl. Sci.* **10**, 197–223 (1988)
59. Niezgodka, M., Songmu, Z., Sprekels, J.: Global solutions to a model of structural phase transitions in shape memory alloys. *J. Math. Anal. Appl.* **130**, 39–54 (1988)
60. Oswald, P.: *Multilevel Finite Element Approximation*. Stuttgart: Teubner (1994)
61. Pawłow, I.: Three-dimensional model of thermomechanical evolution of shape memory materials. *Control Cybern.* **29**, 341–365 (2000)
62. Pego, R.L.: Phase transitions in one-dimensional nonlinear viscoelasticity: admissibility and stability. *Arch. Ration. Mech. Anal.* **97**, 353–394 (1987)
63. Plecháč, P.: Computation of microstructure with interfacial energies. In: Bock, H.G. et al. (eds): *ENUMATH 97*. Singapore: World Scientific (1998)
64. Plecháč, P., Roubíček, T.: Visco-elasto-plastic model for martensitic phase transformation in shape-memory alloys. *Math. Methods Appl. Sci.* **25**, 1281–1298 (2002)
65. Rajagopal, K.R., Roubíček, T.: On the effect of dissipation in shape-memory alloys. *Nonlinear Anal. Real World Appl.* **4**, 581–597 (2002)
66. Rajagopal, K.R., Srinivasa, A.R.: On the thermomechanics of shape memory wires. *Z. Angew. Math. Phys.* **50**, 459–496 (1999)
67. Raniecki, B., Lexcellent, C., Tanaka, K.: Thermodynamic model of pseudoelastic behavior of shape memory alloys. *Arch. Mech.* **44**, 261–284 (1992)
68. Ren, X., Truskinovsky, L.: Finite scale microstructures in nonlocal elasticity. *J. Elasticity* **59**, 319–355 (2000)
69. Rogers, R., Truskinovsky, L.: Discretization and hysteresis. *Physica B* **233**, 370–375 (1997)
70. Roubíček, T.: *Relaxation in Optimization Theory and Variational Calculus*. Berlin: De Gruyter (1997)
71. Roubíček, T.: Dissipative evolution of microstructure in shape memory alloys. In: Bungartz, H.J., Hoppe, R.H.W., Zenger, C. (eds): *Lectures on Applied Mathematics*. Berlin: Springer, pp. 45–63 (2000)
72. Rybka, P.: Dynamical modelling of phase transitions by means of viscoelasticity in many dimensions. *Proc. R. Soc. Edinb. Sect. A* **121**, 101–138 (1992)
73. Rybka, P., Hoffmann, K.H.: Convergence of solutions to the equation of quasi-static approximation of viscoelasticity with capillarity. *J. Math. Anal. Appl.* **226**, 61–81 (1998)
74. Sauter, S.A.: Variable order panel clustering. *Computing* **64**, 223–261 (2000)
75. Schneider, R.: *Multiskalen- und Wavelet-Matrixkompression: Analysisbasierte Methoden zur effizienten Lösung großer vollbesetzter Gleichungssysteme*. Advances in Numerical Mathematics. Stuttgart: Teubner (1998)
76. Simo, J.C.: A framework for finite strain elastoplasticity based on maximum plastic dissipation and the multiplicative decomposition. *Comput. Methods Appl. Mech. Eng.* **66**, 199–219 and **68**, 1–31 (1988)
77. Sprekels, J.: Global existence for thermomechanical processes with nonconvex free energies of Ginzburg-Landau form. *J. Math. Anal. Appl.* **141**, 333–348 (1989)
78. Swart, P.J., Holmes, P.J.: Energy minimization and the formation of microstructure in dynamic anti-plane shear. *Arch. Ration. Mech. Anal.* **121**, 37–85 (1992)
79. Sweldens, W.: The lifting scheme: A construction of second generation wavelets *SIAM J. Math. Anal.* **29**, 511–546 (1998)
80. Truskinovsky, L.: Transition to detonation in dynamic phase changes. *Arch. Ration. Mech. Anal.* **125**, 375–397 (1994)
81. Tyrtshnikov, E.: Mosaic-skeleton approximations. *Calcolo* **33**, 470–57 (1996)
82. Vainchtein, A., Rosakis, P.: Hysteresis and stick-slip motion of phase boundaries in dynamic models of phase transitions. *J. Nonlinear Sci.* **9**, 697–719 (1999)